1 **Title page**

2 **SLC19A1 is a cyclic dinucleotide transporter**

3

4 **Rutger D. Luteijn[1], Shivam A. Zaver[2], Benjamin G. Gowen[3,4], Stacia Wyman[3,4], Nick Garelis[1],**

5 **Liberty Onia[1], Sarah M. McWhirter[5], George E. Katibah[5], Jacob E. Corn[3,4,†], Joshua J.**

6 **Woodward[2], David H. Raulet[1*]**

7
8 [1]Department of Molecular and Cell Biology, and Cancer Research Laboratory, Division of

9 Immunology and Pathogenesis, University of California, Berkeley, CA, 94720, USA

10

11 [2]Department of Microbiology, University of Washington, Seattle, WA, 98195, USA

12 [3]Innovative Genomics Initiative, University of California, Berkeley, Berkeley, CA, 94720, USA

13 [4]Department of Molecular and Cell Biology, University of California, Berkeley, Berkeley, CA,

14 94720, USA

15 [5]Aduro Biotech, Inc. Berkeley, CA, 94710, USA

16 [†]current address: HPL, Otto-Stern-Weg 7, ETH Zurich, 8093 Zurich, Switzerland

17

18 *correspondence:

19 raulet@berkeley.edu

20 tel: 510-642-9521
21
22
23

24

The accumulation of DNA in the cytosol serves as a key immunostimulatory signal associated with infections, cancer and genomic damage[1,2]. Cytosolic DNA triggers immune responses by activating the cGAS/STING pathway[3]. The binding of DNA to the cytosolic enzyme cGAMP synthase (cGAS), activates its enzymatic activity, leading to the synthesis of a second messenger, cyclic[G(2',5')pA(3',5')] (2'3'-cGAMP)[4–8]. 2'3'-cGAMP, a cyclic dinucleotide (CDN), activates the protein 'stimulator of interferon genes' (STING)[9], which in turn activates the transcription factors IRF3 and NF-κB promoting the transcription of genes encoding type I interferons and other cytokines and mediators that stimulate a broader immune response. Exogenous 2'3'-cGAMP and other CDNs, including CDNs produced by bacteria and synthetic CDNs used in cancer immunotherapy, must traverse the cell membrane to activate STING in target cells. How these charged CDNs pass through the lipid bilayer is unknown. Here we used a genome-wide CRISPR interference screen to identify the reduced folate carrier SLC19A1 as the major CDN transporter for uptake of synthetic and naturally occurring CDNs. CDN uptake and functional responses are inhibited by depleting SLC19A1 from cells and enhanced by overexpressing *SLC19A1*. In both cell lines and primary cells *ex vivo*, CDN uptake is inhibited competitively by folate and blocked by the SLC19A1 inhibitor sulfasalazine, a medication approved for the treatment of inflammatory diseases. The identification of SLC19A1 as the major transporter of CDNs into cells has far reaching implications for the immunotherapeutic treatment of cancer[10], transport of 2'3'-cGAMP from tumor cells to other immune cells to trigger the anti-tumor immune response[11], host responsiveness to CDN-producing pathogenic microorganisms[12], and potentially in certain inflammatory diseases.

Main text

The cGAS/STING pathway senses cytosolic DNA originating from viruses and bacteria[9] as well as CDNs produced by certain bacteria[13–15]. Notably, the STING pathway is also activated by cytosolic self DNA, which accumulates in cells in certain autoinflammatory disorders, including Aicardi–Goutieres Syndrome and systemic lupus erythematosus[16–19]. Furthermore, cytosolic DNA

52 accumulates in cells subjected to DNA damage, as occurs in tumor cells, resulting in activation of the

53 cGAS/STING pathway and the initiation of an anti-tumor immune response[20]. Recently, we revealed

54 that 2'3'-cGAMP can be transferred from tumor cells to immune cells *in vivo*, prompting the

55 activation of the immune response[11]. Furthermore, synthetic STING agonists, such as 2'3'-RR CDA,

56 an analogue of 2'3'-cGAMP (Fig. S1)[21], can greatly enhance the anti-tumor immune response when

57 delivered directly into the tumor microenvironment in mouse models of cancer, causing tumor

58 regressions[10,22]. 2'3'-RR CDA and other synthetic CDNs are currently being tested in clinical trials as

59 cancer immunotherapies. However, a critical outstanding question is the mechanism of transport of

60 CDNs into cells of the immune system[23]. CDNs may be incorporated into cells via gap junctions,

61 membrane fusions, or by incorporation into viral particles[24–27,28]. but none of these mechanisms

62 explain (systemic) immune activation by extracellular CDNs. To systematically identify the genes

63 involved in cytosolic transport of CDNs, we performed a genome-wide CRISPR interference screen

64 in the monocytic THP-1 cell line.

65   To visualize STING activation, THP-1 cells were transduced with a CDN-inducible reporter

66 construct (Fig. 1a). The reporter was composed of Interferon Stimulatory Response Elements (ISRE)

67 and a mouse minimal IFN-β promoter that drives the expression of tdTomato upon hIFN-β or CDN

68 exposure (Fig. 1b). In line with previous results, the synthetic CDN 2'3'-RR CDA induced a more

69 potent response than 2'3'-cGAMP[10] even when applied at a lower concentration. The response to

70 both CDNs was several fold higher than the response to hIFN-β, and was completely dependent on

71 STING expression (Fig. 1b), implying that the reporter primarily reported cell-intrinsic STING

72 activity. To interrogate the approximately 20,000 human genes for their role in CDN-induced reporter

73 expression, we performed a genome-wide CRISPR interference (CRISPRi) forward genetic screen in

74 THP-1 cells. We generated a stable line of THP-1 cells expressing dCas9-BFP-KRAB, which was

75 validated and expanded before transducing the cells with the CRISPRi v2 library at a low multiplicity

76 of infection (see Methods). The CRISPRi library of cells was stimulated either with 2'3'-RR CDA, or

77 with 2'3'-cGAMP, using concentrations that resulted in 90% reporter-positive cells. The highest

78 expressing 25% and lowest expressing 25% of stimulated cells in each library were sorted by flow

79 cytometry, DNA isolated, and gRNA sequences from each population, and unsorted cells, were

80 amplified and DNA from each of these populations as well as from unsorted cells was deep-

81 sequenced to identify the targeted genes in each population (Fig. 1c and Fig. S2). The fold enrichment

82 and depletion of gRNAs in the hypo-responsive population versus the hyper-responsive population

83 was calculated for each screen (Fig. S3, Table S1 and Table S2). We also integrated multiple gRNAs

84 per gene using Mageck (see Methods) comparing the hyporesponsive and hyperresponsive

85 populations calculated as robust rank aggregations scores and depicted in Fig. 1d and e. Similar

86 results were obtained when each sorted population was compared to unsorted cells (Table S2). The

87 two screens yielded many common hits, but there were some differences, such as numerous hits in the

88 2'3'-cGAMP screen including STAT2, IRF9, IFNAR1, and IFNAR2 (Table S2). Hence, the 2'3'-RR

89 CDA screen may have been mostly dependent on intrinsic STING signaling, whereas the 2'3'-

90 cGAMP screen may have been partly dependent on autocrine/paracrine IFN-β signaling.

91   In both CDN screens, the top hits in the hypo-responsive population (i.e. the genes most

92 important for robust responses to CDNs) included the transcription factor IRF3, which acts directly

93 downstream of STING. One of the five gRNAs for STING itself was also enriched in hyporesponsive

94 cells from both screens, though the other STING gRNAs were not, presumably because they were

95 ineffective at interfering with STING expression (Table S1). Other significant hits included genes

96 involved in transcription, splicing, and immune modulation (Table S2).

97   One of the most significant hits in both screens was the *SLC19A1* gene. SLC19A1 is a cell

98 surface transporter known as the reduced folate carrier. SLC19A1 and another transporter, SLC46A1,

99 are responsible for uptake of folate from the extracellular environment[29]. To validate the role of

100 *SLC19A1* in CDN stimulation, the top two enriched *SLC19A1*-targeting gRNAs from the 2'3'-RR

101 CDA screen were used to stably deplete *SLC19A1* in THP-1 cells expressing dCas9-KRAB (Fig.

102 S4a). *SLC19A1*-depleted cells grew normally and appeared healthy, suggesting that other folate

103 transport mechanisms fully suffice in *SLC19A1*-deficient cells. *SLC19A1*-depleted and, for

104 comparison, *IRF3*-depleted cells (Fig. S4b) were stimulated with 2'3'-cGAMP, 2'3'-RR CDA, cyclic

105 [A(3',5')pA(3',5')] (3'3' CDA, a bacterial CDN) or hIFN-β, and reporter induction was measured 20

106 h later (Fig. 2a). Responses to 2'3'-cGAMP, 2'3'-RR CDA and 3'3'-CDA were each strongly

107   inhibited in *IRF3*- and *SLC19A1*-depleted cells (Fig. 2b), whereas stimulation by hIFN-β was not

108   affected (Fig. 2b). Restoration of *SLC19A1* expression by transduction of a cDNA expression vector

109   rescued CDN responsiveness without affecting stimulation by hIFN-β (Fig. 2c).

110   As an alternative approach to corroborate the role of *SLC19A1* in CDN responses, the

111   conventional CRISPR/Cas9 system was used to target a coding exon in order to generate loss of

112   function mutations in the *SLC19A1* gene. Disruption of the *SLC19A1* gene was confirmed by genomic

113   PCR, TA-cloning and sequencing for nine *SLC19A1*^{-/-} clones (see Methods). These clones were all

114   significantly less sensitive to CDN stimulation when compared to seven control clones that received a

115   non-targeting gRNA (Fig. 2d).

116   Importantly, *SLC19A1* overexpression robustly increased CDN responsiveness in THP-1 cells

117   as well as in cell lines that normally responded poorly or not at all to CDN stimulation, including

118   C1R, K562, 293T (pre-transduced with STING), and RAW macrophage cell lines (Fig. 2e and f).

119   Taken together, our data show reduced responses to CDNs in *SLC19A1*-deficient cells and much

120   amplified responses in cells overexpressing *SLC19A1*, as might be expected for a CDN transporter.

121   Together, these data support a central role of the SLC19A1 transporter in responses to several cyclic

122   dinucleotides, including the mammalian CDN 2'3'-cGAMP.

123   Based on our findings, we tested whether the drug sulfasalazine (SSZ), a non-competitive

124   inhibitor of SLC19A1[30], would block stimulation by CDNs. THP-1 reporter cells were exposed to

125   various concentrations of SSZ or DMSO vehicle in the presence of 2'3'-cGAMP, 2'3'-RR CDA, or

126   hIFN-β. Responses to both CDNs were robustly inhibited with increasing concentrations of SSZ,

127   whereas responses to hIFN-β stimulation were only modestly inhibited (Fig. 2g). The concentrations

128   required for inhibition were only modestly higher than those that inhibit uptake of folate derivatives in

129   another study[30]. Surprisingly, at lower concentrations, SSZ modestly enhanced stimulation by 2'3'-

130   RR CDA, but had no effect on stimulation by 2'3' cGAMP (Fig. 2g).

131   The effect of SLC19A1 on reporter induction by CDNs led us to test the impact of SLC19A1

132   deficiency on endogenous transcriptional targets downstream of STING, including the genes encoding

133   the chemokines CCL5 and CXCL10, which are direct targets of IRF3[31,32]. In control cells, *CCL5* and

134   *CXCL10* gene expression was highly elevated 5h after 2'3'-RR CDA stimulation. In cells depleted of

135 *IRF3*, *SLC19A1* or *STING*, chemokine expression was strongly inhibited, indicating that SLC19A1

136 action is necessary for CDN-induced effects, including those downstream of STING (Fig. 3a and b).

137   To directly assess the effect of SLC19A1 on STING pathway activation (Fig. S5), we

138 evaluated phosphorylation of STING, IRF3 and TBK1 in control (non-targeting gRNA) versus

139 CRISPRi-depleted cells by immunoblotting (Fig. 3c). Within 2 hours after stimulation with 2'3'-RR

140 CDA, phosphorylation of STING, IRF3, and TBK1 were each significantly elevated in control THP-1

141 cells. In *IRF3*-depleted cells, phosphorylation of upstream signaling components STING and TBK1

142 was not affected, whereas in *STING*-depleted cells phosphorylation of both TBK1 and IRF3 was

143 nearly ablated. *SLC19A1*-targeted cells showed major defects in phosphorylation of STING, TBK1

144 and IRF3, supporting the conclusion that *SLC19A1* acts upstream of STING. Notably, protein levels

145 of STING, TBK1, and IRF3 were unaltered in *SLC19A1*-depleted cells, indicating that SLC19A1 does

146 not influence stability or degradation of STING pathway components.

147   To further exclude a general defect in STING activation caused by *SLC19A1*-depletion, the

148 cGAS/STING pathway was directly triggered intracellularly by transfecting cells with interferon

149 stimulatory DNA (ISD). ISD transfection of both WT and *SLC19A1*-depleted THP-1 cells resulted in

150 a strong and equal induction of *IFNB* gene expression (Fig. 3d). Thus, STING functioned normally in

151 *SLC19A1*-depleted cells when DNA was introduced directly into the cytosol by transfection.

152   The finding that *SLC19A1* was not essential when DNA was transfected into cells suggested

153 that SLC19A1 may function by transporting CDNs into cells. Therefore, we enzymatically

154 synthesized [^{32}P] 2'3'-cGAMP, which we confirmed by TLC and DRaCALA[33] binding analysis (Fig.

155 S6a and b). We next monitored 2'3'-cGAMP uptake by cells expressing different levels of SLC19A1.

156 SLC19A1 overexpression greatly enhanced uptake of [^{32}P] 2'3'-cGAMP by THP-1 cells (Fig. 4a) and

157 C1R cells (Fig. S7a). Conversely, *SLC19A1*-depletion reduced the uptake of ^{32}P 2'3'-cGAMP in

158 THP-1 cells (Fig. 4a). We next sought to determine the specificity for 2'3'-cGAMP uptake in THP-1

159 cells. Addition of excess, unlabeled bacterial-derived 3'3'-linked cyclic di-nucleotides as well as host-

160 derived 2'3'-cGAMP to cell culture media completely inhibited [^{32}P] 2'3'-cGAMP uptake by THP-1

161 cells, suggesting that cyclic di-nucleotide interactions with the transporter are not highly specific for

162 the 2'3' linkage or the specific nucleotides (Fig. 4b). In quantitative competition ligand uptake assays,

163   unlabeled 2'3'-cGAMP inhibited uptake of [^{32}P] 2'3'-cGAMP with an IC$_{50}$ of 1.89 ± 0.11 µM, in line

164   with the reported affinity of SLC19A1 for methotrexate and other folates (Fig. 4c)[34]. As SLC19A1

165   was first described as a folate transporter, we performed similar competition experiments using

166   excess, unlabeled folic acid, and we also tested an inhibitor of folate uptake by SLC19A1,

167   sulfasalazine. Remarkably, both folic acid and sulfasalazine inhibited [^{32}P] 2'3'-cGAMP uptake with

168   IC$_{50}$'s of 4.79 ± 0.08 µM and 2.06 ± 0.17 µM, respectively (Fig. 4d and e). We extended the study by

169   asking whether folic acid or sulfasalazine inhibited uptake of [^{32}P] 2'3'-cGAMP in other cell types.

170   We found that the addition of excess folate and sulfasalazine to cell cultures abrogated [^{32}P] 2'3'-

171   cGAMP uptake by U937 monocytes as well as primary murine peritoneal leukocytes and splenocytes

172   (Fig. 4f, S7b). Taken together these results suggested that uptake of the mammalian CDN 2'3'-

173   cGAMP by human and mouse cells, including cell lines and primary cell *ex vivo*, depends on

174   SLC19A1 expression and function.

175   If SLC19A1 transports CDNs into cells, CDNs may directly interact with SLC19A1.

176   Consistent with a direct interaction between 2'3'-cGAMP and SLC19A1, His-tagged SLC19A1 was

177   precipitated by 2'3'-cGAMP immobilized on Sepharose beads (Fig. 4g and S8). This interaction was

178   specific, as free, unbound 2'3'-cGAMP competitively disrupted the 2'3'-cGAMP-SLC19A1

179   interaction (Fig. 4h and S8). As a positive control, His-tagged STING C-terminal domain was also

180   precipitated by 2'3'-cGAMP-Sepharose (Fig 4g and S8). These data suggest that CDNs interact with

181   SLC19A1, consistent with the proposed role of SLC19A1 as a CDN transporter. Taken together, our

182   results demonstrate that SLC19A1 is a mammalian CDN transporter, required for exogenous CDN-

183   mediated type I Interferon activation.

184   The response to CDNs is weak in most cell lines tested, and can be increased by overexpression

185   of *SLC19A1*. Indeed, THP-1 cells are near the top of a large set of cell lines in expression of both

186   *SLC19A1* and *STING* (Fig. S9), suggesting that *SLC19A1* expression and *STING* expression may

187   together predict the responsiveness to CDN stimulation by cell lines and tumors.

188   Both folic acid and sulfasalazine almost completely blocked CDN uptake and/or stimulation,

189   whereas CDN stimulation was not completely inhibited in *SLC19A1*-null cells. This implied that

190   another transporter sensitive to folic acid competition and sulfasalazine inhibition may play a role in

191   CDN uptake. Overexpression of *SLC46A1*, which encodes the only other known folate transporter,

192   did increase responses to CDNs (Fig. S10). However, depletion of *SLC46A1* had only a modest effect

193   on CDN stimulation, and was not a significant hit in our screen. Furthermore, depleting *SLC46A1* and

194   *SLC19A1* together was no more effective than depleting SLC19A1 alone (Fig. S11). These data

195   suggest that yet another transporter that is inhibited by folic acid and sulfasalazine may play a partial

196   role in CDN transport. SLC46A3, another transporter, was also a hit in our screen. Overexpression of

197   *SLC46A3* increased the response to CDNs (Fig. S10). Depletion of *SLC46A3* had a modest effect on

198   reporter induction by both CDNs (Fig. S11). However, depleting both *SLC19A1* and *SLC46A3*

199   together did not reduce responses more than depletion of *SLC19A1* alone (Fig. S11), suggesting that

200   SLC46A3 is not responsible for most of the residual CDN transport in *SLC19A1*-depleted cells.

201   Our findings define SLC19A1 as a major transporter of exogenous 2'3' cGAMP, 2'3'-RR CDA

202   and probably other CDNs into the cytosol. In this context, it likely plays an important role in the anti-

203   tumor and adjuvant effects of injected CDNs. It may also be important in cell-to-cell transport of

204   CDNs in immune responses, both in the context of cancer[11] and potentially during viral infections.

205   SLC19A1-mediated uptake of CDNs may also be critical for the pathology of various inflammatory

206   diseases[35,36]. For example, in mouse models of inflammatory bowel disease (IBD), some evidence

207   suggests that host cells import CDNs produced by intestinal bacteria, activating STING in a cGAS-

208   independent fashion[36]. SLC19A1-mediated uptake of CDNs from the extracellular environment may

209   thus contribute to the inflammatory profile underlying such diseases. Moreover, the SLC19A1

210   inhibitor sulfasalazine is a first line treatment in rheumatoid arthritis, and is often used to treat

211   inflammatory bowel diseases (IBD), including ulcerative colitis and Crohn's disease[37,38].

212   Sulfasalazine has an immunosuppressive effect, in part by inhibiting the NF-κB pathway[39], but the

213   mechanism of inhibition is unknown. Our results raise the intriguing possibility that sulfasalazine

214   exerts its anti-inflammatory effects in these diseases by inhibiting uptake of CDNs produced

215   endogenously or by commensal bacteria, preventing STING activation. In conclusion, we have

216   identified SLC19A1 as a CDN transporter with potential relevance in the context of cancer

217   immunotherapy, immunosurveillance, and inflammatory disease.

218

219 **Methods**

220

221 **Cell culture**

222 All cell lines were cultured at 37°C in humidified atmosphere containing 5% CO2 with media

223 supplemented with 100 U/mL penicillin, 100 μg/mL streptomycin, 0.2 mg/mL glutamine, 10 μg/mL

224 gentamycin sulfate, 20 mM Hepes and 10% FCS. THP-1, C1R, and K562 cells were cultured in

225 RPMI medium, and 293T, 293T transfected with hSTING (293T+hSTING), MDA-MBA-453

226 (MDA), and RAW macrophages were cultured in DMEM medium. THP-1, K562, 293T cells, and

227 RAW macrophages were present in the lab at the time this study began. MDA cells were obtained

228 from the Berkeley Cell Culture Facility. C1R cells were a generous gift from Veronika Spies (Fred

229 Hutchinson Cancer Center, Seattle WA). 293T+hSTING cells were generated at Aduro Biotech Inc.

230

231 **Antibodies and reagents**

232 The following antibodies were derived from Cell signaling technologies: rabbit-anti-human TBK1

233 mAb (clone D1B4, used 1:500 for immunoblot [IB]), rabbit-anti-human phospho-TBK1 mAb (clone

234 D52C2, 1:1000 for IB), rabbit-anti-human STING mAb (clone D2P2F, 1:2000 for IB), rabbit-anti-

235 human phospho STING mAb (clone D7C3S, used 1:1000 for IB), rabbit-anti-human phospho-IRF3

236 mAb (clone 4D4G, 1:1000 for IB). Antibodies derived from LI-COR Biosciences: goat-anti-mouse

237 IgG IRDye 680RD conjugated (cat. #: 926-68070, used 1:5000), donkey-anti-rabbit IgG IRDye

238 800CW conjugated (cat. #: 926-32213), donkey-anti-rabbit IgG IRDye 680RD (cat. #: 926-68073).

239 Other antibodies: rabbit-anti-human IRF3 mAb (Abcam, cat. #: EP2419Y, used 1:2000 for IB),

240 mouse-anti-human transferrin receptor mAb (Thermo Fischer Scientific, clone H68.4, used 1:1000 for

241 IB), rabbit-ant-human SLC19A1 pAb (Picoband, cat. #: PB9504, used 0.4 μg/ml for IB), APC-

242 conjugated mouse-anti-human CD55 mAb (BioLegend, clone JS11, used 1:50 for flow cytometry),

243 mouse-anti-human CD59 mAb (BioLegend clone p282, used 1:250 for flow cytometry), APC-

244 conjugated goat-anti-mouse IgG (BioLegend, cat. #: 405308, used 1:100 for flow cytometry).

245 Reagents used: Sulfasalazine (Sigma-Aldrich, cat. #: S0883), polybrene (EMD Millipore, cat. #:

246 TR1003G), 3'3'-cyclic-di-AMP (CDA) (Invivogen, cat. #: tlrl-nacda), 2'3'-RR CDA and 2'3'- cyclic-

247   di-GMP-AMP (cGAMP) (generous gift from Aduro Bioscience Inc.), human interferon-β

248   (PeproTech, cat. #: 300-02B), mouse interferon-β1 (BioLegend, cat. #: 581302). Antibiotic selection:

249   puromycin (Sigma-Aldrich, cat. #: P8833), blasticidin (Invivogen, cat. #: ant-bl-1, used at 10 µg/ml),

250   zeocin (Invivogen, cat. #: ant-zn-1, used at 200 µg/ml).

251

252   **Plasmids**

253   A gBLOCK gene fragment (Integrated DNA Technologies, Inc.) encoding the tdTomato reporter gene

254   driven by the interferon stimulatory response elements (ISREs) and the minimal mouse interferon-β

255   promoter was cloned into a dual promoter lentiviral plasmid by means of Gibson assembly. This

256   lentiviral plasmid co-expressed the Zeocin resistance gene and GFP via a T2A ribosomal skipping

257   sequence controlled by the human EF1A promoter, and was generated as described previously[40].

258   For rescue and overexpression of *SLC19A1*, *SLC46A1*, or *SLC46A3*, a gBLOCK gene fragment

259   encoding *SLC19A1* (gene ID 6573, transcript 1), *SLC46A1* (gene ID 113235) or *SLC46A3* (gene ID

260   283537) was cloned by Gibson assembly into a dual promoter lentiviral plasmid co-expressing the

261   Blasticidin resistance gene and the fluorescent gene mAmetrine.

262   For CRISPR interference (CRISPRi)-mediated depletions, cells were transduced with a lentiviral

263   dCas9-HA-BFP-KRAB-NLS expression vector (Addgene plasmid #102244).

264   For screen validation using individual gRNAs, gRNAs (table S3) were cloned into the same

265   expression plasmid used for the gRNA library ("pCRISPRia-v2", Addgene plasmid #84832, a gift

266   from Jonathan Weissman). The lentiviral gRNA plasmid co-expresses a puromycin resistance gene

267   and blue fluorescence protein (BFP) via a T2A ribosomal skipping sequence controlled by the human

268   EF1A promoter. The CRISPRi gRNAs introduced into this vector by Gibson assembly were

269   expressed from a murine U6 promoter. For expression of multiple gRNAs, additional gRNAs were

270   introduced in a separate vector that co-expressed the blasticidin resistance gene and mAmetrine via a

271   T2A ribosomal skipping sequence under the control of a human EF1A promoter.

272   Conventional CRISPR gRNAs (see table S3) were cloned into a selectable lentiviral CRISPR/Cas9

273   vector. This lentiviral vector includes a human codon-optimized *S.pyogenes* Cas9 co-expressing

274 puromycin resistance gene via a T2A ribosome skipping sequence under the control of a minimal

275 human EF1A promoter[40,41].

276

277 **Lentiviral production and transduction**

278 Lentivirus was produced by transfecting lentiviral plasmids and 2nd generation packaging/polymerase

279 plasmids into 293T cells using TransIT-LT1 Reagent (Mirus Bio LLC). Virus-containing supernatants

280 were harvested 72h later, centrifuged to remove cell debris, and filtered using a 0.45 µm PES filter.

281 Filtered virus supernatant was used to transduce target cells by spin-infection (800 x g for 90min at

282 33°C) in the presence of 8 µg/ml polybrene. After spin-infection virus and polybrene containing

283 medium was diluted 1:1 with fresh medium. 72 hours after transduction, cells were sorted based on

284 fluorescence expression using a BD FACSAria cell sorter, or selected with relevant selection reagent.

285

286

287 **2'3'-RR CDA and 2'3'-cGAMP screens**

288 THP-1 cells co-expressing the tdTomato reporter, GFP, and dCas9-BFP were single cell sorted to

289 select for a THP-1 cell clone with efficient dCas9-BFP-knockdown capacity. Clonal populations were

290 transduced with lentiviral vectors encoding gRNAs targeting GFP, *CD55* or *CD59*. After 1 week on

291 puromycin (2 µg/ml) selection, CD55, CD59 and GFP expression were quantified using the BD LSR

292 Fortessa flow cytometer. A clonal cell that showed the highest reduction in all three marker genes was

293 selected for the screens. Two cultures of THP-1 cells were separately transduced with the human

294 genome-wide CRISPRi v2 library[42]. Each library of THP-1 cells was separately screened by treating

295 the cells with 2'3'-RR CDA or 2'3'-cGAMP followed by selection and analysis. Hence, each screen

296 was performed twice, with different CRISPRi library transduced cultures of THP-1 cells.

297 For each transduction, the THP-1 clone was expanded to 320 million cells and transduced

298 with the human genome-wide CRISPRi v2 library[42], which contains approximately 100,000 gRNAs

299 targeting around 20,000 genes. Sufficient cells were transduced and propagated to maintain at least 50

300 million transduced (BFP+) cells, representing 500x coverage of the gRNA library. The transduction

301 efficiency was around 20% to minimize the chance of multiple lentiviral integrations per cell. Two

302 days after transduction, cells were cultured in the presence of puromycin for two days and one day

303 additional day without puromycin. 400 million cells were seeded to a density of 1 million cells/ml and

304 stimulated with 2'3'-RR CDA (2 μg/ml) or 2'3'-cGAMP (15 μg /ml). 20h later, cells were harvested,

305 washed in PBS, and sorted based on BFP expression (presence of gRNAs), GFP expression (presence

306 of reporter) and tdTomato expression using the BD Influx cell sorter and BD FACSaria Fusion cell

307 sorter. The cells were sorted into two populations based on tdTomato expression: the highest 25% of

308 tdTomato expressing cells (hyper-responsive population) and lowest 25% of tdTomato expressing

309 cells (hypo-responsive population). During sorting, all cells were kept at 4°C. After sorting, cells were

310 counted: the sorted populations contained 15-20 million cells, and the unsorted control contained 100-

311 150 million cells. Cells were washed in PBS, and cell pellets were stored at -80°C until further

312 processing.

313

314 **gDNA isolation and sequencing**

315 Genomic DNA was isolated from sorted cells using NucleoSpin Blood kits (Macherey-Nagel). PCR

316 was used to amplify gRNA cassettes with Illumina sequencing adapters and indexes as described

317 previously[43]. Genomic DNA samples were first digested for 18 hours with *SbfI*-HF (NEB) to liberate

318 a ~500 bp fragment containing the gRNA cassette. The gRNA cassette was isolated by gel

319 electrophoresis as described previously[43]. using NucleoSpin Gel and PCR Clean-up kits (Macherey-

320 Nagel), and the DNA was then used for PCR. Custom PCR primers are listed in Supplementary Table

321 5. Indexed samples were pooled and sequenced on an Illumina HiSeq-2500 for the 2'3'RR CDA

322 screen and an Illumna HiSeq-4000 for the 2'3'-cGAMP screen using a 1:1 mix of two custom

323 sequencing primers (Supplementary Table 5). Sequencing libraries were pooled proportional to the

324 number of sorted cells in each sample. The target sequencing depth was at least 2,000 reads/gRNA in

325 the library for unsorted "background" samples, and at least 10 reads/cell in sorted samples.

326

327 **Screen data analysis**

328 CRISPRi samples were analyzed using the Python-based ScreenProcessing pipeline

329 (https://github.com/mhorlbeck/ScreenProcessing). Normalization using a set of negative control genes

330 and calculation of phenotypes and Mann-Whitney *p-value*s was performed as described

331 previously[42,44]. Briefly, Illumina 50bp single end sequencing reads for pooled sublibraries one to four

332 and five to seven were trimmed to 29bp and guides were quantified by counting exact matches to the

333 CRISPRi v2 human library guides. Phenotypes were calculated as the log2 fold change in enrichment

334 of an sgRNA in the high and low samples versus background as well as high versus low, normalized

335 by median subtracting non-targeting sgRNAs[44,45]. Phenotypes from sgRNAs targeting the same gene

336 were collapsed into a single sensitivity phenotype for each gene using the average of the top three

337 scoring sgRNAs (by phenotype absolute value). For genes with multiple independent transcription

338 start sites (TSSs) targeted by the sgRNA libraries, phenotypes and *p-value*s were calculated

339 independently for each TSS and then collapsed to a single score by selecting the TSS with the lowest

340 Mann-Whitney *p-value*. Counts from the ScreenProcessing pipeline were then used as input to the

341 MAGeCK program to obtain FDR scores for filtering (see table S2).

342

343 Genes were also ranked by individual gRNAs with the greatest enrichment/depletion between the

344 hypo-responsive and hyper-responsive libraries. gRNA read counts were normalized to library

345 sequencing depth by converting to read counts per million total reads. For each gRNA, the ratio

346 between the read counts for the hypo-responsive and hyper-responsive libraries was found and

347 averaged between replicates. For hypo-responsive gene rankings, each gene was ranked by the single

348 corresponding gRNA with the highest hypo-to-hyper ratio (see table S1, 'highest ratio hypo/hyper'

349 column). For hyper-responsive gene rankings, each gene was ranked by the single corresponding

350 gRNA with the lowest hypo-to-hyper ratio (see table S1, 'lowest ratio hypo/hyper' column). Gene-

351 level phenotypes are available as Supplemental Materials (table S1 and S2).

352

353 **CDN and IFN-β Stimulation assays**

354 The week prior to stimulation experiments, cells were cultured at the same density. The day before

355 stimulation, cells were seeded to 0.5×10^5 cells/ml. Cells were stimulated with CDNs or IFN- β in 48W

356 plates using 50,000 cells/well in 300 µl medium. After 18-24h, cells were transferred to a 96W plate

357 and tdTomato expression was measured by flow cytometry using a high throughput plate reader on a

358　BD LSR Fortessa. For stimulations in the presence of sulfasalazine, cells were stimulated in 48W

359　plates using 20,000 cells/well in 300 µl medium. Cells were incubated with sulfasalazine or DMSO as

360　vehicle prior to stimulations with CDNs or IFN-β. 18-24h after stimulation, tdTomato reporter

361　expression was quantified by flow cytometry using a high throughput plate reader on a BD LSR

362　Fortessa.

363

364　**Production of SLC19A1 knockout cell lines**

365　THP-1 cells expressing the tdTomato reporter were transduced with a CRISPR/Cas9 lentiviral

366　plasmid encoding a control gRNA or a gRNA targeting *SLC19A1* at a region critical for transport[46]

367　(see table S3). Transduced cells were selected using puromycin for 2 days and single cell sorted using

368　a BD FACSAria cell sorter. Control cells and *SLC19A1*-targeted cells were selected that had

369　comparable forward and side scatter by flow cytometry analysis. Genomic DNA was isolated from

370　clones using the Qiamp DNA minikit (Qiagen), and the genomic region surrounding the *SLC19A1*

371　gRNA target site was amplified by PCR using primers 5'-TTCTCCACGCTCAACTACATCTC-3'

372　and 5'-CAGCATCCGCGCCAGCACTGAGT-3'. PCR product was cloned into 5-alpha competent

373　bacteria (New England Biolabs, cat. #C2987) using a TOPO TA cloning kit (Thermo Fischer

374　Scientific, cat. # 450641) according to manufacturer's instructions. After blue/white screening, a

375　minimum of 10 colonies were sequenced per THP-1 clone, and sequences were analyzed using

376　SeqMan (Lasergene DNASTAR). THP-1 clones with out-of-frame mutations at the SLC19A1 gRNA

377　target site were selected for further experiments.

378

379　**RT-qPCR**

380　Cells were harvested and washed in ice-cold PBS. Cells were transferred to RNase-free

381　microcentrifuge tubes and RNA was isolated using the RNeasy mini kit (Qiagen, cat. #: 74104)

382　including a DNase step (Qiagen, cat. #: 79254). RNA concentration was measured by NanoDrop

383　(Thermo Fischer), and 1 µg of RNA was used as input for cDNA synthesis using the iScript cDNA

384　synthesis kit (Bio-rad, cat. #: 1708890). cDNA was diluted to 20 ng/µl and 2.5 µl/reaction was used

385　as input for the qPCR reaction. qPCR reactions were set up using SSOFast EvaGreen Supermix (Bio-

386   Rad, cat. #: 1725200) according to the manufacturer's recommendations, using 500 nM of each

387   primer and following cycling conditions on a Bio-Rad C1000 Thermal Cycler: 2 min at 98°C, 40

388   repeats of 2 sec at 98°C and 5 sec at 55°C. Primers used to amplify the *HPRT1, YHWAZ, CCL5,*

389   *CXCL10*, *STING*, *IRF3*, *SLC19A1*, *SLC46A1*, and *SLC46A3*-specific PCR products are listed in table

390   S4. The housekeeping genes *HPRT1* and *YHWAZ* served as endogenous control.

391   For quantification of *IFNB1* mRNA, RNA was extracted with the Nucleospin RNA Isolation Kit

392   (Machery-Nagel) and reverse-transcribed with the iScript cDNA synthesis kit (Bio-Rad). TaqMan

393   real-time qPCR assays were used for quantification of human *IFNB1* (Hs01077958_s1). *ACTB*

394   (Hs01060665_g1) served as an endogenous control.

395

396   **Synthesis of [^{32}P] cyclic GMP-AMP and [^{32}P] cyclic di-AMP**

397   Radiolabeled 2'3' cGAMP was enzymatically synthesized by incubating 0.33 μM α-[^{32}P] ATP

398   (Perkin-Elmer) with 250 μM unlabeled GTP, 1 μg of Interferon Stimulatory DNA 100mer (kindly

399   provided by Daniel Stetson), and 1 μM of recombinant His-tagged 2'3' cGAMP Synthase (cGAS) in

400   binding buffer [40 mM Tris pH 7.5, 100 mM NaCl, 20 mM MgCl$_2$] at 37°C overnight. The reaction

401   was confirmed to have gone to completion by Thin Layer Chromatography (TLC) analysis. Briefly,

402   the 2'3' cGAMP synthesis reaction was separated on Polygram CEL300 PEI TLC plates (Machery-

403   Nagel) in buffer containing 1:1.5 (vol/vol) saturated (NH$_4$)$_2$SO$_4$ and 1.5 M NaH$_2$PO$_4$ pH 3.6. The TLC

404   plates were then air dried and exposed to a PhosphorImager screen for visualization using a Typhoon

405   scanner (GE Healthcare Life Sciences). Next, the sample was incubated with HisPur Ni-NTA resin

406   (Thermo Scientific) for 30 min in order to remove recombinant cGAS. The resultant slurry was

407   transferred to a minispin column (Thermo Scientific) to elute crude [^{32}P] 2'3' cGAMP. Recombinant

408   mSTING-CTD protein was used for further purification of synthesized [^{32}P] 2'3' cGAMP. 100 μM

409   mSTING-CTD was bound to HisPur Ni-NTA resin and incubated with the remaining crude 2'3'

410   cGAMP synthesis reaction mixture for 30 min on ice. Following removal of the supernatant, the Ni-

411   NTA resin was washed three times with cold binding buffer. The resin was then incubated with 100

412   μL of binding buffer for 10 min at 95 °C, and transferred to a minispin column to elute [^{32}P] 2'3'

413   cGAMP. The resulting STING-purified [^{32}P] 2'3' cGAMP was evaluated by TLC analysis and

414   determined to be ~99% pure.

415   Radiolabeled c di-AMP was synthesized as described previously [47]. Briefly, 1 μM α-[^{32}P] ATP

416   (Perkin-Elmer) was incubated with 1 μM of recombinant DisA in binding buffer at 37°C overnight.

417   The reaction mixture was boiled for 5 min at 95°C and DisA was removed by centrifugation.

418   Recombinant His-tagged RECON was then used to further purify the c di-AMP reaction mixture. 100

419   μM His-tagged RECON was bound to HisPur Ni-NTA resin for 30 min on ice. The resin was washed

420   three times with cold binding buffer and then incubated with 100 μL of binding buffer for 5 min at

421   95°C. The slurry was then transferred to a minispin column to elute [^{32}P] c di-AMP. The purity of the

422   radiolabeled c di-AMP was assessed by TLC and determined to be ~98%.

423

424   **Nucleotide-Binding Assays**

425   The ability of radiolabeled 2'3' cGAMP and c di-AMP to bind recombinant STING was evaluated by

426   DRaCALA (differential radial capillary action of ligand assay) analysis, as previously described[48].

427   Briefly, varying concentrations of recombinant STING were incubated with ~1 nM of radiolabeled

428   cyclic di-nucleotide in binding buffer for 10 min at room temperature. The reaction mixtures were

429   blotted on nitrocellulose membranes and air dried for 15 min. The membranes were then exposed to a

430   PhosphorImager screen and visualized using a Typhoon scanner.

431

432   **Nucleotide-Uptake Assays**

433   For transport assays, cells were collected by centrifugation and washed in Dulbecco's Phosphate-

434   Buffered Saline (DPBS) (Life Technologies). The cell pellets were re-suspended in pre-warmed

435   RPMI 1640 medium (GIBCO) containing 10% heat-inactivated FBS (HyClone) and supplemented

436   with 10 mM HEPES, 1 mM sodium pyruvate and 2 mM L-Glutamine (Thermo Fisher) to a final cell

437   density of 1 X 10^7 cells per ml. Uptake of 1 nM [^{32}P] cGAMP and c di-AMP was assayed in cell

438   suspensions at 37°C over the indicated time points. At the end of each time point, transport was

439   quenched by the addition of cold DPBS. Cells were washed three times with cold DPBS, followed by

440 lysis in 50 μL of cold deionized water. The cell lysates were then transferred to 5 ml of liquid

441 scintillation cocktail (National Diagnostics) and the associated radioactivity was measured by liquid

442 scintillation counting using a LS6500 Liquid Scintillation Counter (Beckman Coulter). For each

443 sample, $[^{32}P]$ cyclic di-nucleotide uptake (counts per minute) was normalized to cell count. For

444 competition experiments, cells were pre-incubated with indicated concentrations of "cold" unlabeled

445 ligand for 15 minutes prior to the addition of 1 nM "hot" $[^{32}P]$ cGAMP. Cells were then collected at

446 the indicated time points and processed as described above.

447

448 **Protein Expression and Purification**

449 Full-length human SLC19A1 cDNA with a C-terminal 8 X His-tag was subcloned into a dual

450 promoter lentiviral vector (see above). Recombinant His-tagged SLC19A1 was expressed using a

451 FreeStyle 293 Expression System. Briefly, 293F cells (1 X 10^6 cells per ml) grown in FreeStyle 293

452 Media supplemented with GlutaMax (GIBCO) were transfected with the SLC19A1 expression

453 construct (1μg plasmid DNA per ml of cells) using PEI transfection reagent. Transfected cells were

454 grown for 72 hours in a shaking incubator at 37°C in 5% CO_2. Three days after transfection, the cells

455 were harvested by centrifugation and washed in DBPS. Cell pellets were then re-suspended in lysis

456 buffer [25 mM Tris pH 8.0, 150 mM NaCl, 1 mM phenylmethylsulfonyl fluoride] supplemented with

457 HALT Protease and Phosphatase Inhibitor Cocktail (Thermo Scientific) and lysed by sonication. The

458 cell lysate was supplemented with 2% (w/v) n-dodecyl-β-D-maltoside (DDM) and rotated for 2h at

459 4°C. The cell lysates were centrifuged at 15,000 rpm for 1h at 4°C to remove cell debris, and the

460 detergent-soluble fraction was incubated with HisPur Ni-NTA resin for 1h at 4°C. The resin was

461 washed with 100 column volumes of wash buffer [25 mM Tris pH 6.0, 150 mM NaCl, 30 mM

462 imidazole, 5% glycerol (v/v), and 0.05% DDM (w/v)], and bound proteins were eluted in elution

463 buffer [25 mM Tris pH 6.0, 150 mM NaCl, 300 mM imidazole, 5% glycerol (v/v), and 0.05% DDM

464 (w/v)]. The resulting proteins were analyzed by SDS-PAGE followed by Coomasie staining and

465 immunoblotting to confirm expression and purification of His-tagged SLC19A1.

466

467   Recombinant cGAS, DisA, mSTING-CTD, and mRECON were expressed and purified as previously

468   described[47–49]. Briefly, plasmids for cGAS, DisA, mSTING-CTD, and mRECON expression were

469   transformed into Rosetta (DE3) pLysS chemically competent cells. Overnight cultures of the resulting

470   transformed bacteria were inoculated into 1.5 L of LB broth at a 1:100 dilution. Bacterial cultures

471   were grown at 37°C to OD_{600} 0.5 followed by overnight induction at 18°C with 0.5 mM isopropyl β-

472   D-1-thiogalactopyranoside (IPTG). Cells were harvested and lysed in PBS supplemented with 1 mM

473   PMSF and soluble protein was purified using nickel-affinity chromatography followed by gel

474   filtration chromatography (S-300, GE Healthcare, Piscataway, New Jersey, USA). After SDS-PAGE

475   analysis, the purified proteins were concentrated in storage buffer [40 mM Tris pH 7.5, 100 mM

476   NaCl, 20 mM $MgCl_2$, 25% glycerol (v/v)] and stored at -80°C.

477

478   **Synthesis of cGAMP Sepharose**

479   2'3' cyclic GMP-AMP was enzymatically synthesized using recombinant cGAS as described

480   previously[8,48]. Approximately, 100 mg of purified cGAMP was dissolved in PBS to 200 μM. The pH

481   of the solution was adjusted to 7.5 with NaOH, and the resulting solution was added directly to

482   washed epoxy-activated Sepharose and incubated at 56°C for 2 days. The Sepharose was washed and

483   the absorbance spectrum of 50% slurry was measured to ensure nucleotide coupling. HPLC analysis

484   of the remaining uncoupled nucleotide ensured no degradation of cGAMP occurred during the 2-day

485   incubation. The remaining epoxy groups were blocked with ethanolamine following the instructions

486   provided by GE. In parallel with this blocking step, fresh epoxy-activated Sepharose was also treated

487   with ethanolamine to generate control resin.

488

489   **cGAMP Pulldowns**

490   Following nickel affinity purification, recombinant His-tagged SLC19A1 was incubated with 100 μL

491   of ethanolamine- or cGAMP-conjugated Sepharose beads for 4h at 4°C with rotation, as described

492   previously (Sureka et. al., 2014; McFarland et. al., 2016). Beads were washed three times with wash

493   buffer [25 mM Tris pH 6.0, 150 mM NaCl, 5% glycerol (v/v), and 0.05% DDM (w/v)], and bound

494   proteins were eluted by boiling in SDS-PAGE sample loading buffer for 5 min at 95°C. The soluble

495   fraction was then removed and analyzed by SDS-PAGE followed by Coomassie Blue staining and

496   immunoblotting. As a control, recombinant His-tagged mSTING-CTD was incubated with

497   ethanolamine- or cGAMP-conjugated sepharose beads, as described above. Beads were washed three

498   times with binding buffer, and then boiled in SDS-PAGE sample loading buffer for 5 min at 95°C.

499   The soluble fraction was then analyzed by SDS-PAGE followed by Coomasie staining.

500

501   **Cell lysis and immunoblotting**

502   For anti-SLC19A1 immunoblotting, cells were lysed and proteins were separated by SDS-PAGE as

503   described above in the 'cGAMP pulldowns' paragraph. SDS-PAGE-separated proteins were

504   transferred onto nitrocellulose membranes (Bio-Rad) at 30V overnight at 4°C. Membranes were then

505   air dried for 1h and blocked in 5% Blotto, non-fat milk (NFM, Santa Cruz Biotechnology) in 1 X

506   TBS. Membranes were probed in 5% Bovine Serum Albumin (Fisher) in 1 X TBS-T with anti-

507   SLC19A1 Picoband antibody (Boster Bio).

508   For protein detection using all other antibodies, cells were counted, washed with PBS and

509   lysed in RIPA buffer (25 mM Tris-HCl pH 7.5, 150 mM NaCl, 1 mM EDTA, 1% NP-40, 0.1% SDS)

510   including cOmplete ULTRA protease inhibitors (Sigma-Aldrich cat. #: 05892791001), phosphatase

511   inhibitors (Biomake, cat. # B15001) and 50mM DTT. Cells lysates were mixed with 4x NuPage LDS

512   sample buffer (Invitrogen cat. #: NP0007), pulse sonicated and incubated at 75°C for 5min. Lysates

513   were loaded onto Bolt 4-12% Bis-Tris Plus SDS-PAGE gels (Invitrogen cat. #: NW04125BOX).

514   SDS-PAGE separated proteins were transferred onto Immobilon-FL PVDF membranes (EMD

515   Millipore) at 100V for 1h at 4°C. Membranes were blocked in 4% NFM, and probed in 1% NFM

516   overnight at 4°C with primary antibody. Membranes were subsequently washed 3 times in 1x-TBS-T

517   and probed with secondary antibody for 1h at RT protected from light. Membranes were washed 2

518   times in TBS-T, once in TBS, and blots were imaged using an Odyssey CLx System (LI-COR).

519

520   **Mice**

521 C57BL/6J mice were obtained from The Jackson Laboratory. All of the mice were maintained in

522 specific pathogen free conditions by the Department of Comparative Medicine at the University of

523 Washington School of Medicine. All experimental procedures using mice were approved by the

524 Institutional Animal Care and Use Committee of the University of Washington and were conducted in

525 accordance with institutionally approved protocols and guidelines for animal care and use.

526

527 **Isolation of Mouse Peritoneal Cavity Cells and Splenocytes**

528 Mouse peritoneal cavity cells were recovered by peritoneal lavage with 5 ml ice cold PBS

529 supplemented with 3% FCS, as previously described[50]. The peritoneal cells were cultured in RPMI

530 1640 medium (GIBCO) supplemented with 10% (v/v) heat-inactivated FBS (HyClone), 10 mM

531 HEPES, 1 mM sodium pyruvate, 2 mM L-Glutamine (Thermo Fisher), 100 U/ml penicillin, 100

532 μg/ml streptomycin at 37°C in the presence of 5% CO_2.

533 For isolation of murine splenocytes, spleens were removed from mice, strained through a 70

534 μm cell strainer, and homogenized into a single cell suspension using ice cold PBS supplemented

535 with 3% FCS. Red blood cells were lysed by resuspending spleen cells in Red Blood Cell Lysing

536 Buffer (Sigma) and incubating on ice for 10 min. Splenocytes were washed, resuspended in RPMI

537 1640 medium (GIBCO) supplemented with 10% (v/v) heat-inactivated FBS (HyClone), 10 mM

538 HEPES, 1 mM sodium pyruvate, 2 mM L-Glutamine (Thermo Fisher), 100 U/ml penicillin, 100

539 μg/ml streptomycin, and used immediately for [^{32}P] cGAMP uptake assays.

540

541

542 **References**

543

544 1.   Ishii, K. J. *et al.* A toll-like receptor-independent antiviral response induced by double-

545   stranded B-form DNA. *Nat. Immunol.* **7,** 40–48 (2006).

546 2.   Stetson, D. B. & Medzhitov, R. Recognition of cytosolic DNA activates an IRF3-dependent

547   innate immune response. *Immunity* **24,** 93–103 (2006).

548 3.   Li, T. & Chen, Z. J. The cGAS–cGAMP–STING pathway connects DNA damage to

549   inflammation, senescence, and cancer. *J. Exp. Med.* **215,** 1287–1299 (2018).

550   4.   Zhang, X. *et al.* Cyclic GMP-AMP containing mixed Phosphodiester linkages is an

551   endogenous high-affinity ligand for STING. *Mol. Cell* **51,** 226–235 (2013).

552   5.   Sun, L., Wu, J., Du, F., Chen, X. & Chen, Z. J. Cyclic GMP-AMP synthase is a cytosolic

553   DNA sensor that activates the type I interferon pathway. *Science* **339,** 786–91 (2013).

554   6.   Gao, P. *et al.* Cyclic [G(2′,5′)pA(3′,5′)p] is the metazoan second messenger produced by DNA-

555   activated cyclic GMP-AMP synthase. *Cell* **153,** 1094–1107 (2013).

556   7.   Ablasser, A. *et al.* CGAS produces a 2′-5′-linked cyclic dinucleotide second messenger that

557   activates STING. *Nature* **498,** 380–384 (2013).

558   8.   Diner, E. J. *et al.* The Innate Immune DNA Sensor cGAS Produces a Noncanonical Cyclic

559   Dinucleotide that Activates Human STING. *Cell Rep.* **3,** 1355–1361 (2013).

560   9.   Ishikawa, H. & Barber, G. N. STING is an endoplasmic reticulum adaptor that facilitates

561   innate immune signalling. *Nature* **455,** 674–8 (2008).

562   10.   Corrales, L. *et al.* Direct Activation of STING in the Tumor Microenvironment Leads to

563   Potent and Systemic Tumor Regression and Immunity. *Cell Rep.* **11,** 1018–30 (2015).

564   11.   Marcus, A. *et al.* Tumor-Derived cGAMP Triggers a STING-Mediated Interferon Response in

565   Non-tumor Cells to Activate the NK Cell Response. *Immunity* **49,** 754–763.e4 (2018).

566   12.   McWhirter, S. M. *et al.* A host type I interferon response is induced by cytosolic sensing of the

567   bacterial second messenger cyclic-di-GMP. *J. Exp. Med.* **206,** 1899–1911 (2009).

568   13.   Dey, R. J. *et al.* Inhibition of innate immune cytosolic surveillance by an M.Tuberculosis

569   phosphodiesterase. *Nat. Chem. Biol.* **13,** 210–217 (2017).

570   14.   Woodward, J. J., Lavarone, A. T. & Portnoy, D. A. C-di-AMP secreted by intracellular

571   Listeria monocytogenes activates a host type I interferon response. *Science (80-.).* **328,** 1703–

572   1705 (2010).

573   15.   Barker, J. R. *et al.* STING-dependent recognition of cyclic di-AMP mediates type I interferon

574   responses during Chlamydia trachomatis infection. *MBio* **4,** 1–11 (2013).

575   16.   Lam, A. R. *et al.* RAE1 ligands for the NKG2D receptor are regulated by STING-dependent

576   DNA sensor pathways in lymphoma. *Cancer Res.* **74,** 2193–2203 (2014).

577   17.   Ahn, J., Gutman, D., Saijo, S. & Barber, G. N. STING manifests self DNA-dependent

578   inflammatory disease. *Proc. Natl. Acad. Sci. U. S. A.* **109,** 19386–91 (2012).

579   18.   Gao, D. *et al.* Activation of cyclic GMP-AMP synthase by self-DNA causes autoimmune

580   diseases. *Proc. Natl. Acad. Sci.* **112,** E5699–E5705 (2015).

581   19.   Gall, A. *et al.* Autoimmunity initiates in nonhematopoietic cells and progresses via

582   lymphocytes in an interferon-dependent autoimmune disease. *Immunity* **36,** 120–31 (2012).

583   20.   Woo, S. R. *et al.* STING-dependent cytosolic DNA sensing mediates innate immune

584   recognition of immunogenic tumors. *Immunity* **41,** 830–842 (2014).

585   21.   Corrales, L. & Gajewski, T. F. Molecular Pathways: Targeting the Stimulator of Interferon

586   Genes (STING) in the Immunotherapy of Cancer. *Clin. Cancer Res.* **21,** 4774–9 (2015).

587   22.   Corrales, L., McWhirter, S. M., Dubensky, T. W. & Gajewski, T. F. The host STING pathway

588   at the interface of cancer and immunity. *J. Clin. Invest.* **126,** 2404–11 (2016).

589   23.   Sundararaman, S. K. & Barbie, D. A. Tumor cGAMP Awakens the Natural Killers. *Immunity*

590   **49,** 585–587 (2018).

591   24.   Gentili, M. *et al.* Transmission of innate immune signaling by packaging of cGAMP in viral

592   particles. *Science* **349,** 1232–6 (2015).

593   25.   Bridgeman, A. *et al.* Viruses transfer the antiviral second messenger cGAMP between cells.

594   *Science* **349,** 1228–32 (2015).

595   26.   Ablasser, A. *et al.* Cell intrinsic immunity spreads to bystander cells via the intercellular

596   transfer of cGAMP. *Nature* **503,** 530–534 (2013).

597   27.   Xu, S. *et al.* cGAS-Mediated Innate Immunity Spreads Intercellularly through HIV-1 Env-

598   Induced Membrane Fusion Sites. *Cell Host Microbe* **20,** 443–457 (2016).

599   28.   Chen, Q. *et al.* Carcinoma-astrocyte gap junctions promote brain metastasis by cGAMP

600   transfer. *Nature* **533,** 493–498 (2016).

601   29.   Hou, Z. & Matherly, L. H. *Biology of the major facilitative folate transporters SLC19A1 and*

602   *SLC46A1. Current Topics in Membranes* **73,** (Elsevier Inc., 2014).

603   30.   Jansen, G. *et al.* Sulfasalazine is a potent inhibitor of the reduced folate carrier: Implications

604   for combination therapies with methotrexate in rheumatoid arthritis. *Arthritis Rheum.* **50,**

605   2130–2139 (2004).

606   31.   Lin, R., Heylbroeck, C., Genin, P., Pitha, P. M. & Hiscott, J. Essential Role of Interferon

607   Regulatory Factor 3 in Direct Activation of RANTES Chemokine Transcription. *Mol. Cell.*

608   *Biol.* **19,** 959–966 (1999).

609   32.   Brownell, J. *et al.* Direct, Interferon-Independent Activation of the CXCL10 Promoter by NF-

610   B and Interferon Regulatory Factor 3 during Hepatitis C Virus Infection. *J. Virol.* **88,** 1582–

611   1590 (2014).

612   33.   Donaldson, G. P., Roelofs, K. G., Luo, Y., Sintim, H. O. & Lee, V. T. A rapid assay for

613   affinity and kinetics of molecular interactions with nucleic acids. *Nucleic Acids Res.* **40,**

614   (2012).

615   34.   Zhao, R., Diop-Bove, N., Visentin, M. & Goldman, I. D. *Mechanisms of Membrane Transport*

616   *of Folates into Cells and Across Epithelia. Annual Review of Nutrition* **31,** (2011).

617   35.   King, K. R. *et al.* IRF3 and type i interferons fuel a fatal response to myocardial infarction.

618   *Nat. Med.* **23,** 1481–1487 (2017).

619   36.   Ahn, J., Son, S., Oliveira, S. C. & Barber, G. N. STING-Dependent Signaling Underlies IL-10

620   Controlled Inflammatory Colitis. *Cell Rep.* **21,** 3873–3884 (2017).

621   37.   Plosker, G. L. & Croom, K. F. Sulfasalazine: a review of its use in the management of

622   rheumatoid arthritis. *Drugs* **65,** 1825–49 (2005).

623   38.   Kozuch, P. L. & Hanauer, S. B. Treatment of inflammatory bowel disease: A review of

624   medical therapy. *World J. Gastroenterol.* **14,** 354–377 (2008).

625   39.   Wahl, C., Liptay, S., Adler, G. & Schmid, R. M. Sulfasalazine: A potent and specific inhibitor

626   of nuclear factor kappa B. *J. Clin. Invest.* **101,** 1163–1174 (1998).

627   40.   van de Weijer, M. L. *et al.* A high-coverage shRNA screen identifies TMEM129 as an E3

628   ligase involved in ER-associated protein degradation. *Nat. Commun.* **5,** 3832 (2014).

629   41.   van Diemen, F. R. *et al.* CRISPR/Cas9-Mediated Genome Editing of Herpesviruses Limits

630   Productive and Latent Infections. *PLoS Pathog.* **12,** e1005701 (2016).

631   42.   Horlbeck, M. A. *et al.* Compact and highly active next-generation libraries for CRISPR-

632   mediated gene repression and activation. *Elife* **5,** 1–20 (2016).

633   43.   Kampmann, M., Bassik, M. C. & Weissman, J. S. Functional genomics platform for pooled

634   screening and generation of mammalian genetic interaction maps. *Nat. Protoc.* **9,** 1825–47

635   (2014).

636   44.   Gilbert, L. A. *et al.* Genome-Scale CRISPR-Mediated Control of Gene Repression and

637   Activation. *Cell* **159,** 647–661 (2014).

638   45.   Kampmann, M., Bassik, M. C. & Weissman, J. S. Integrated platform for genome-wide

639   screening and construction of high-density genetic interaction maps in mammalian cells. *Proc.*

640   *Natl. Acad. Sci.* **110,** E2317–E2326 (2013).

641   46.   Sadlish, H., Williams, F. M. R. & Flintoff, W. F. Functional Role of Arginine 373 in Substrate

642   Translocation by the Reduced Folate Carrier. *J. Biol. Chem.* **277,** 42105–42112 (2002).

643   47.   Huynh, T. N. *et al.* An HD-domain phosphodiesterase mediates cooperative hydrolysis of c-di-

644   AMP to affect bacterial growth and virulence. *Proc. Natl. Acad. Sci. U. S. A.* **112,** E747-56

645   (2015).

646   48.   Sureka, K. *et al.* The cyclic dinucleotide c-di-AMP is an allosteric regulator of metabolic

647   enzyme function. *Cell* **158,** 1389–1401 (2014).

648   49.   McFarland, A. P. *et al.* Sensing of Bacterial Cyclic Dinucleotides by the Oxidoreductase

649   RECON Promotes NF-κB Activation and Shapes a Proinflammatory Antibacterial State.

650   *Immunity* **46,** 433–445 (2017).

651   50.   Ray, A. & Dittel, B. N. Isolation of mouse peritoneal cavity cells. *J. Vis. Exp.* (2010).

652   doi:10.3791/1488

653

654

655   **Data availability**

656   Raw sequencing data from the CRISPRi screen will be deposited to NCBI GEO prior to final

657   publication.

658

659   **Acknowledgements**

675

676   Author contributions

677   RDL, SAZ, and NG performed and analyzed the experiments, LO, SMM, and GEK assisted with the

678   experiments, SW and BGG analyzed the deep-sequencing data and advised on the screen design,

679   RDL, SAZ, BGG, JEC, JW, and DHR designed the experiments, RDL, SAZ, JJW, and DHR prepared

680   the manuscript. All authors critically read the manuscript.

681

682   Competing interests

683   D.H.R. is a co-founder of Dragonfly Therapeutics and served or serves on the scientific advisory

684   boards of Dragonfly, Aduro Biotech, Innate Pharma, and Ignite Immunotherapy; he has a financial

685   interest in all four companies and could benefit from commercialization of the results of this research.

686   SM is, and GK was, an employee of Aduro Biotech.

687

688   **Supplemental information**

689   Supplemental figures S1 to S11

690   Tables S1 to S5

691

692   Table S1. Ranking of target genes based on the ratio between individual gRNAs present in the

693   populations that were hyper-responsive (hyper) or hypo-responsive to CDN treatment (included as

694   Excel file).

695

696   Table S2. Ranking of targeted genes present in the populations hyper-responsive (hyper) or hypo-

697   responsive (hypo) to CDN treatment. RRA ranking is based on the score computed by the MaGeCK

698   program, and phenotypes and p-value calculated by the ScreenProcessing pipeline. (included as Excel

699   file)

700

701   Table S3 guide RNAs

Target gene	gRNA name	sequence (5'-3')	CRISPR system
hIRF3	IRF3-1	GGTCTGCACGGAGAGTGGAA	dCas9-BFP-KRAB
hIRF3	IRF3-2	GGGGTGGACTCCGTAGATGG	dCas9-BFP-KRAB
hSLC19A1	SCL19A1-1	GTACCTGCGACTCGGCGGGG	dCas9-BFP-KRAB
hSLC19A1	SLC19A2-2	GCGGTACCTGCGACTCGGCG	dCas9-BFP-KRAB
hSTING	STING-1	GGCTGCTCTGGATGATGACG	dCas9-BFP-KRAB
hSLC46A1	SLC46A1-1	GTACCGGGCCCCGGCACAGCA	dCas9-BFP-KRAB
hSLC46A3	SLC46A3-1	GGCCGCTGACCGACCGACGG	dCas9-BFP-KRAB
Control	Control	GGAGAGACGGTACCGTCTCA	dCas9-BFP-KRAB
GFP	GFP	GACCAGGATGGGCACCACCC	dCas9-BFP-KRAB
hSLC19A1	SLC19A1	TTCTTCAACCGCGACGACCG	Cas9
Control	Control	GGAGAGACGGTACCGTCTCA	Cas9

702

703 Table S4 qPCR primers

Primer	Sequence (5'-3')
hIRF3 fwd	AGAGGCTCGTGATGGTCAAG
hIRF3 rev	AGGTCCACAGTATTCTCCAGG
hSLC19A1 fwd	TGATCTCGTTCGTGACCTGCT
hSLC19A1 rev	GGCAGACACATTGTCATCAG
hSTING fwd	ACTGTGGGGTGCCTGATAAC
hSTING rev	TGGCAAACAAAGTCTGCAAG
hSLC46A1 fwd	ATGCAGCTTTCTGCTTTGGT
hSLC46A1 rev	GGAGCCACATAGAGCTGGAC
hSLC46A3 fwd	GCCATTCTCTGTTCTACGGTCC
hSLC46A3 rev	GTACCAAGCAACAGTGGCTGAG
hCCL5 fwd	CCTCGCTGTCATCCTCATTG
hCCL5 rev	TGCCACTGGTGTAGAAATACTC
hCXCL10 fwd	CCTTATCTTTCTGACTCTAAGTGGC
hCXCL10 rev	ACGTGGACAAAATTGGCTTG
hHPRT1 fwd	TGACACTGGCAAAACAATGCA
hHPRT1 rev	GGTCCTTTTCACCAGCAAGCT
hYHWAZ fwd	ACTTTTGGTACATTGTGGCTTCAA
hYHWAZ rev	CCGCCAGGACAAACCAGTAT

704
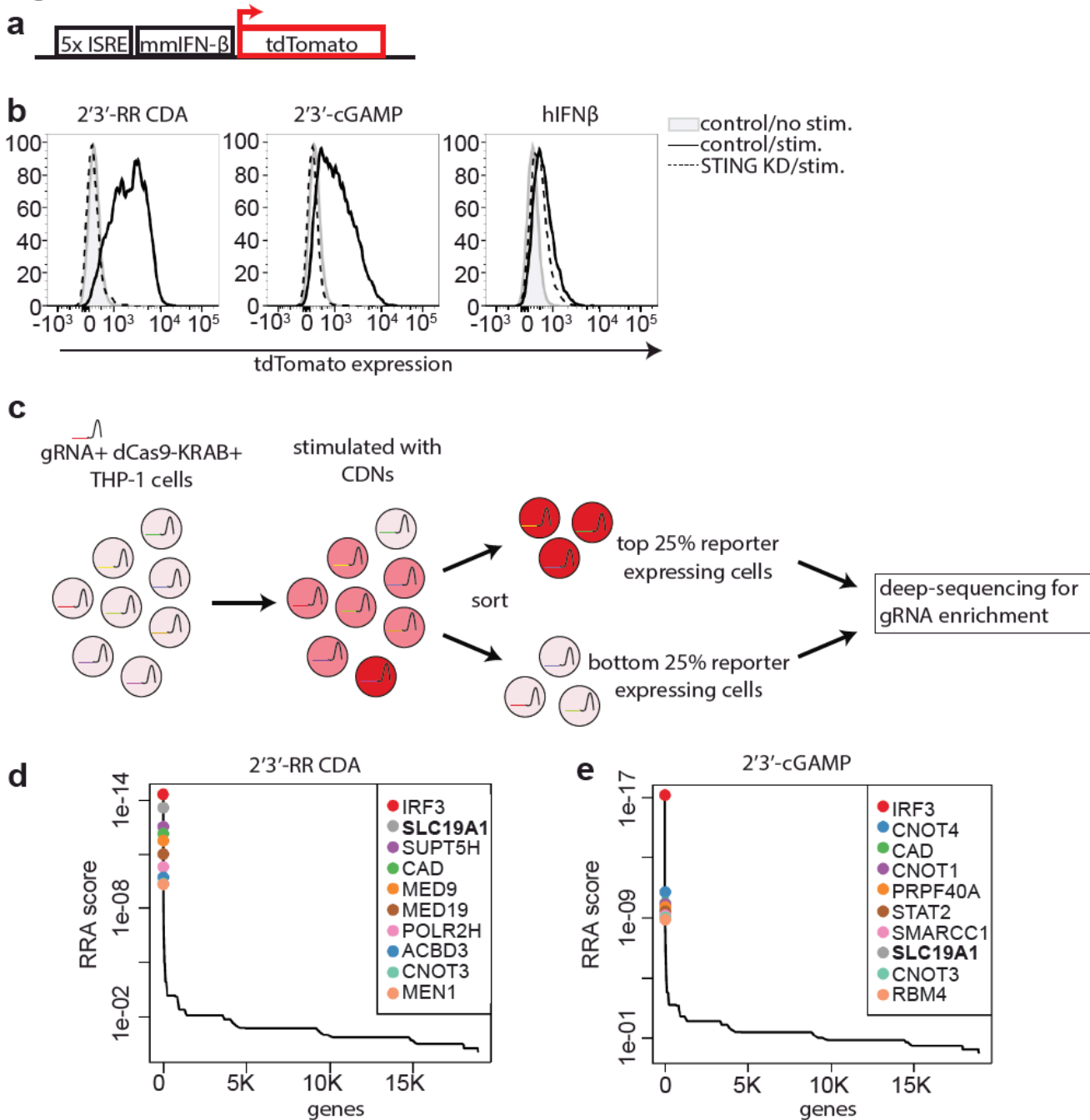
Figure 1. Genome-wide CRISPRi screen for host factors necessary for cyclic dinucleotide (CDN) stimulation. **a,** schematic overview of tdTomato-reporter. tdTomato expression is driven by interferon-stimulatory response elements (ISRE) followed by a mouse minimal interferon beta (mmIFN-β) promoter. **b,** Control THP-1 cells and *STING*-depleted THP-1 cells were incubated with 2'3'-RR CDA (1.67 μg/ml), 2'3'-cGAMP (10 μg/ml) or hIFN-β (100 ng/ml). After 20h, tdTomato reporter expression was analyzed by flow cytometry. Data are representative of three independent experiments with similar results. **c,** Schematic overview of the genome-wide CRISPRi screen. A genome-wide library of CRISPRi guide RNA (gRNA)-expressing THP-1 cells was stimulated with CDNs. 20h after stimulation, cells were sorted into a tdTomato-low group (lowest 25% of cells) and a tdTomato-high group (highest 25% of cells). DNA from the sorted cells was deep sequenced to reveal gRNA enrichment in the two groups. **d-e**, Distribution of the robust rank aggregation (RRA) score in the comparison of hits enriched in the reporter-low versus reporter-high groups of THP-1 cells stimulated with (d) 2'3'-RR CDA or (e) 2'3'-cGAMP. Each panel represents combined results of two independent screens.

Figure 2
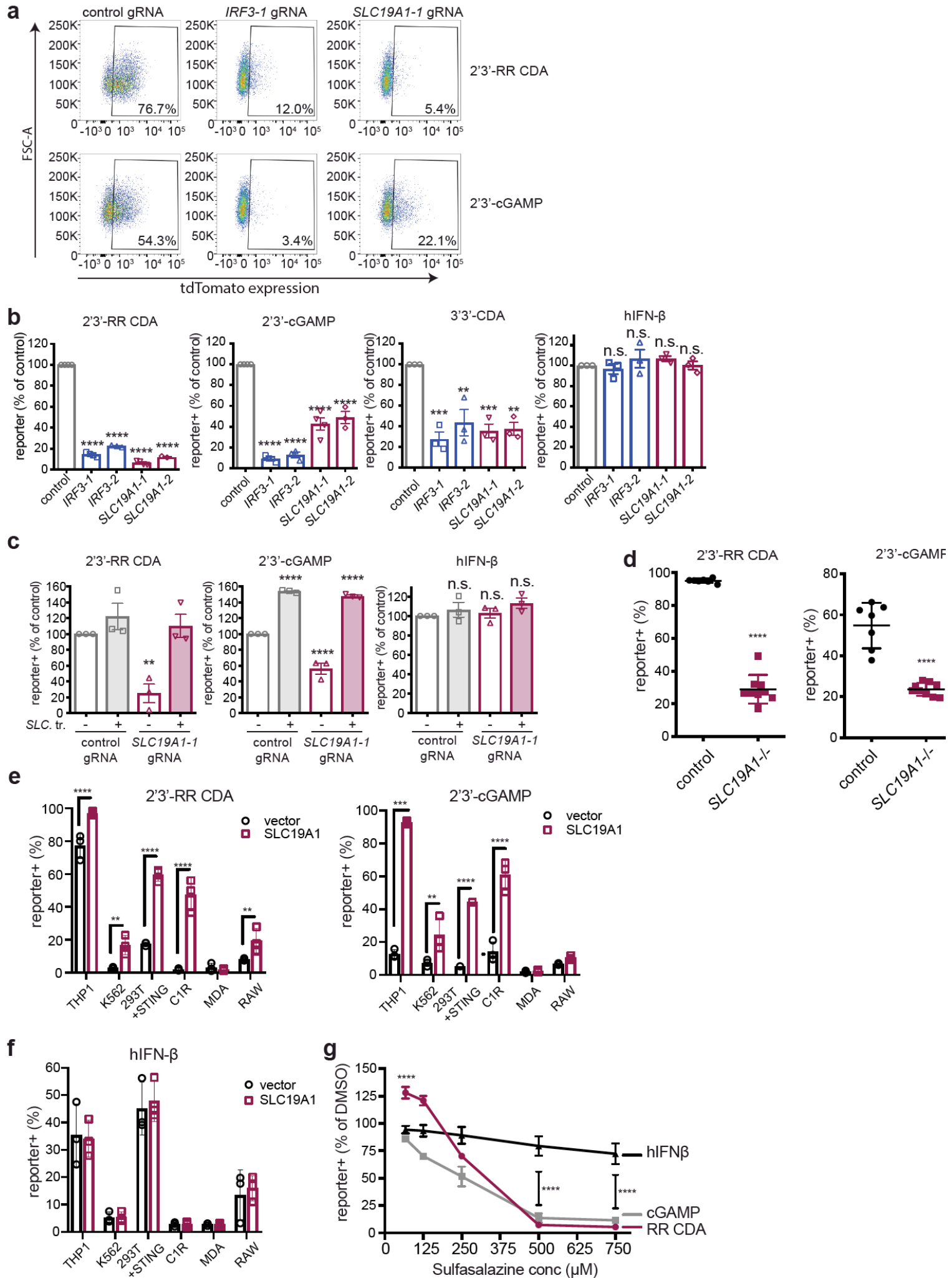
Figure 2. SLC19A1 is required for CDN-induced reporter expression. **a,** dCas9-KRAB-expressing THP-1 cells transduced with non-targeting gRNA (control), *IRF3-1* gRNA or *SLC19A1-1* gRNA were exposed to 2'3'-RR CDA (1.67 μg/ml) or 2'3'-cGAMP (10 μg/ml). 20h later, tdTomato expression was analyzed by flow cytometry. Representative dot plots of three independent experiments are shown. **b,** THP-1 cells expressing the indicated CRISPRi gRNAs or non-targeting gRNA (control), were stimulated with indicated 2'3'-RR CDA (1.67 μg/ml), 2'3'-cGAMP (10 μg/ml), 3'3' CDA (20 μg/ml) or hIFN-β (100 ng/ml). After 18-22h, tdTomato expression was quantified as in (a). Combined results of three independent experiments are shown. **c,** Control THP-1 cells and *SLC19A1-1* gRNA expressing THP-1 cells transduced with *SLC19A1* (SLC. tr.) were exposed to 2'3'-RR CDA (1.67 μg/ml), 2'3'-cGAMP (15 μg/ml) or hIFN-β (100 ng/ml). After 18-22h, tdTomato reporter expression was quantified. Combined results of three independent experiments are shown. **d,** Control THP-1 cells (7 clonal lines) and *SLC19A1*-/- cells (9 clonal lines) were exposed to 2'3'-RR CDA (2.22 μg/ml), 2'3'-cGAMP (10 μg/ml), and tdTomato reporter expression was analyzed by flow cytometry 20h after stimulation. **e,** Various cell lines expressing a control vector or an *SLC19A1* expression vector were stimulated with 2'3'-RR CDA (1.67 μg/ml) or 2'3'-cGAMP (10 μg/ml). After 20h, reporter expression was quantified by flow cytometry. **f,** Various cell lines expressing a control vector or an *SLC19A1* expression vector were stimulated with hIFN-β (100 ng/ml) or murine IFN-β (100 ng/ml) in the case of RAW cells. After 20h, reporter expression was quantified by flow cytometry. **g,** THP-1 cells were incubated with increasing concentrations of 2'3'-RR CDA, 2'3'-cGAMP or hIFN-β in the presence of the SLC19A1 inhibitor sulfasalazine or DMSO as vehicle control. After 18h, tdTomato reporter expression was analyzed by flow cytometry. For each concentration of sulfasalazine, reporter expression in treated cells was compared to reporter expression in cells treated with the same amount of vehicle (DMSO). In panels b and c, e, f, and g, error bars represent ± SEM of three biological replicates. Statistical analysis was performed using one-way ANOVA followed by Tukey's post-test (b and c), unpaired Student's t tests for (d), two-way ANOVA followed by uncorrected Fisher's LSD tests (e and f), and two-way ANOVA followed by Tukey's post-tests to compare the significance between the CDNs and hIFN-β in (g). *$P \leq 0.05$; **$P \leq 0.01$; ***$P \leq 0.001$; ****$P \leq 0.0001$; n.s. not significant
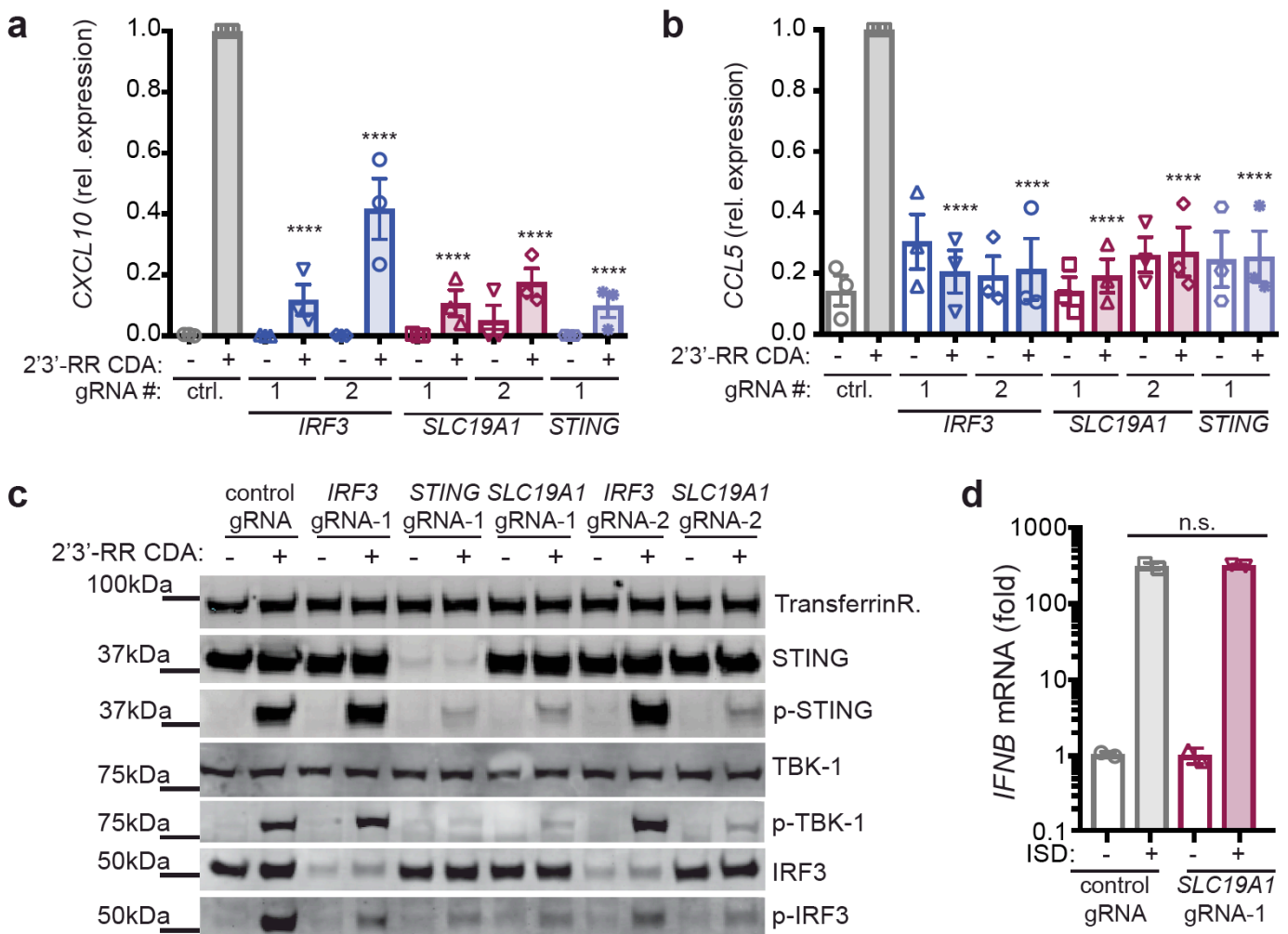
Figure 3

Figure 3. SLC19A1 is critical for STING activation by CDNs. **a, b,** Induction of *CXCL10* (a) or *CCL5* (b) mRNA in control (non-targeting gRNA) THP-1 cells or THP-1 cells expressing the indicated CRISPRi gRNAs after 5h stimulation with 5 μg/ml 2'3'-RR CDA. **c,** Immunoblot analysis of (phospho-) protein expression in control THP-1 cells or THP-1 cells expressing the indicated CRISPRi gRNAs. Cells were stimulated for 2h with 10 μg/ml 2'3'-RR CDA or left unstimulated. TransferrinR.: Transferrin receptor; p-TBK1: TKB1 phosphorylated at position Ser172; p-IRF3: IRF3 phosphorylated at position Ser296; p-STING: STING phosphorylated at position Ser366. Immunoblots are representative of two independent experiments with similar results. **d,** Control THP-1 cells or SLC19A1-depleted THP-1 cells were transfected with 3 μg interferon-stimulatory DNA (ISD) for 3h and the induction of *IFNB* mRNA was measured by RT-qPCR. In panels a, and b: error bars represent ± SEM of at least three biological replicates, In panel d: error bar represents ± SEM of two biological replicates. Statistical analysis was performed using a one-way ANOVA followed by Dunnett's post-test for the comparison of the CDN-stimulated *IRF3*, *SLC19A1*, and *STING*-depleted cell lines to the control CDN-stimulated cells in (a) and an unpaired Student's t test for (d). ****$P \leq 0.0001$; n.s. not significant.

Figure 4
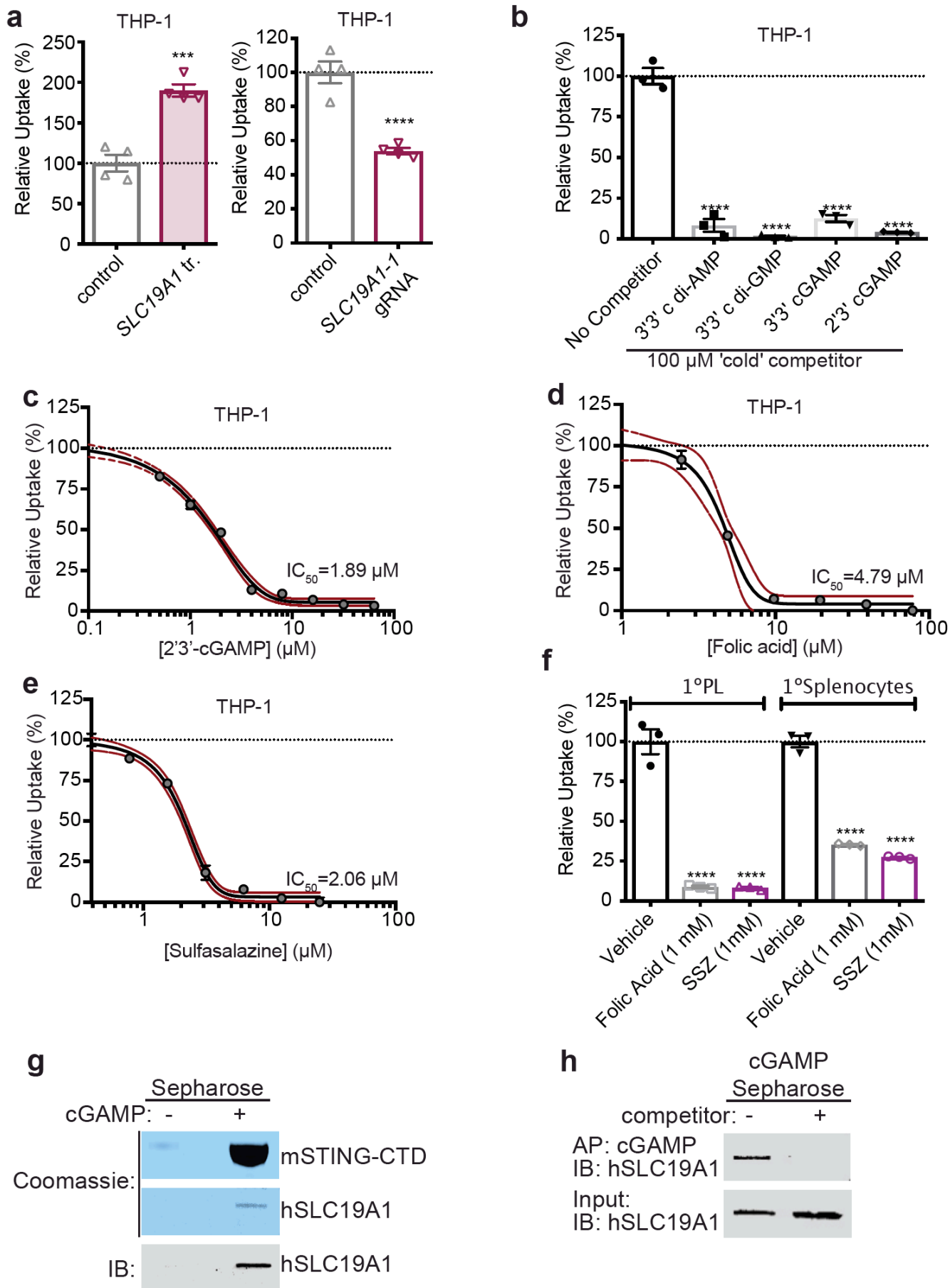
Figure 4. SLC19A1 transports CDNs into cells. **a,** [^{32}P] 2'3'-cGAMP uptake by THP-1 monocytes transduced with empty vector (control) or *SLC19A1* expression vector (left panel), or transduced with a non-targeting control CRISPRi gRNA or *SLC19A1* CRISPRi gRNA (right panel). **b,** [^{32}P] 2'3'-cGAMP uptake by THP-1 monocytes in the presence of 100 μM competing, unlabeled cyclic di-nucleotides. **c, d,** Competitive inhibition of [^{32}P] 2'3'-cGAMP uptake by THP-1 cells in the presence of varying concentrations of competing, unlabeled 2'3'-cGAMP (IC$_{50}$ = 1.89 ± 0.11 μM) or Folic

Acid (IC_{50} = 4.79 ± 0.08 µM). **e,** Inhibition of [^{32}P] 2'3'-cGAMP uptake by THP-1 cells in the presence of varying concentrations of sulfasalazine (IC_{50} = 2.06 ± 0.17 µM). **f,** [^{32}P] 2'3'-cGAMP uptake by primary (1°) peritoneal leukocytes (PL) or splenocytes in the presence of excess folic acid or Sulfasalazine (SSZ). **g,** Binding of SLC19A1 to 2'3' cGAMP. Coomassie staining and Western blot analysis of pulldowns with 2'3' cGAMP-Sepharose (+) or control ethanoloamine-Sepharose (-) beads. The beads were incubated with recombinant C-terminal domain of mSTING (mSTING-CTD) or with recombinant hSLC19A1 before precipitation and analysis. **h,** 2'3'cGAMP competes binding of SLC19A1 to 2'3' cGAMP-Sepharose beads. Soluble 2'3'-cGAMP (250 µM) was added (+) or not (-) to the mixtures of 2'3' cGAMP-Sepharose and hSLC19A1, before precipitation and Western blot analysis. Data are representative of three independent experiments with similar results. Data are representative of three independent experiments with similar results. In all panels, error bars represent ± SEM of biological replicates. Red dashed lines represent the 95% confidence interval for the non-linear regression. Statistical analysis was performed using a Student's t-test (a) or one-way ANOVA (b and f) followed by Tukey's post-test. ***$P \leq 0.001$; ****$P \leq 0.0001$

Figure S1

2'3'-cGAMP

2'3'-RR CDA

3'3'-c-di-AMP

3'3'-c-di-GMP

3'3'-cGAMP
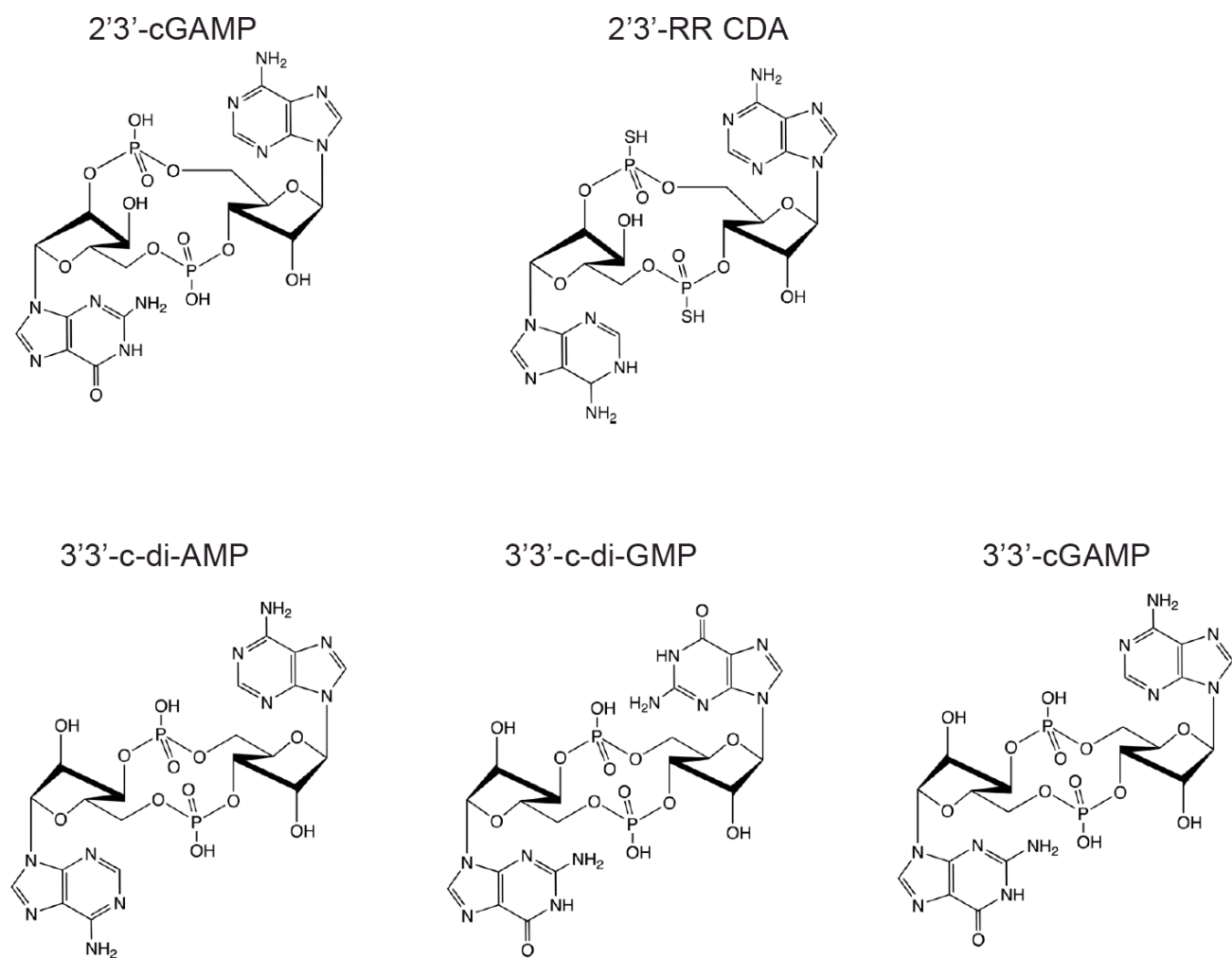
Figure S1. Structures of the CDNs used in this study.

Figure S2
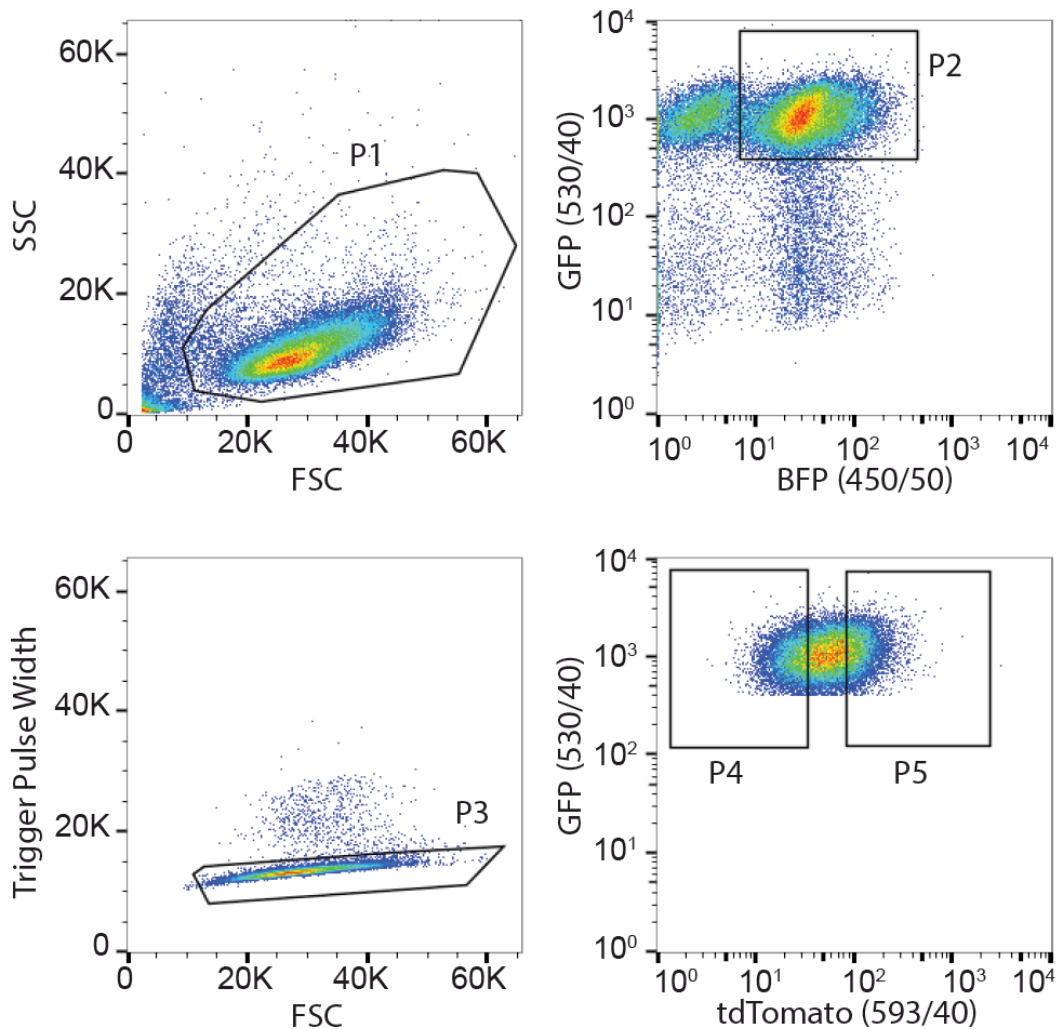
Figure S2. Representative gating strategy for flow cytometry based sorting of the CRISPRi library of reporter-expressing THP-1 cells stimulated with CDNs. Cells were gated based on their forward scatter (FSC) and side scatter (SSC) using gate P1. P1-population was selected based on the expression of blue fluorescent protein (BFP, fluorescent marker for the CRISPRi gRNAs) and GFP (marker for the expression of the reporter construct) using gate P2. In gate P3, the doublet cells present in gate P2 were excluded. In gate P4, population P3 was gated based on tdTomato expression. The lowest 25% of cells expressing tdTomato were selected in gate P4, and the highest 25% of cells expressing tdTomato were selected in gate P5.

Figure S3
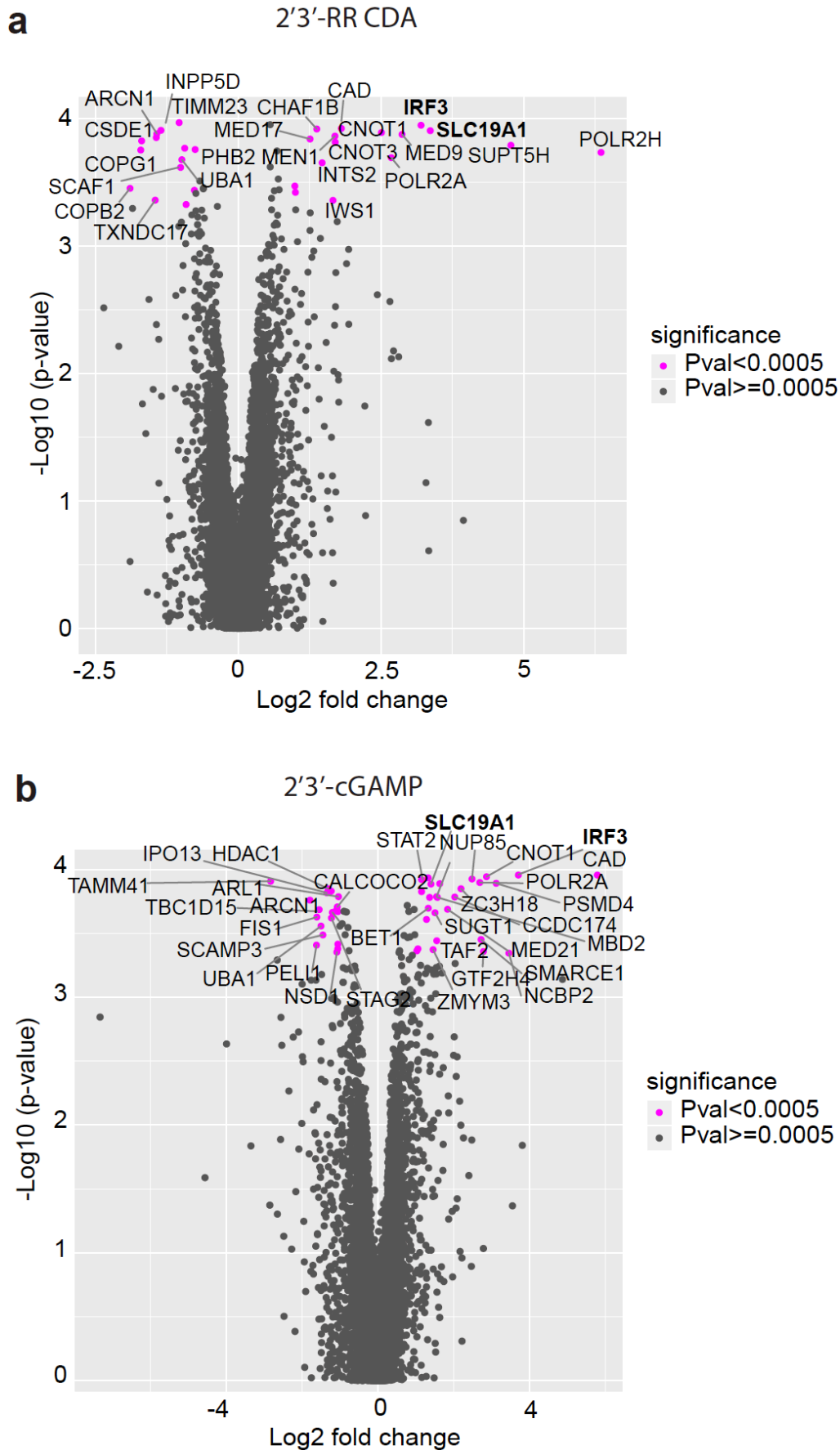
Figure S3. Results of genome-wide CRISPRi screen for host factors crucial for cyclic dinucleotide (CDN) stimulation. Volcano plots of the gRNA-targeted genes enriched or depleted in the tdTomato reporter-low versus reporter-high groups after stimulation with (a) 2'3'-RR CDA or (b) 2'3'-cGAMP. FC: fold change. Each panel represent the combined results of two independent screens.

Figure S4
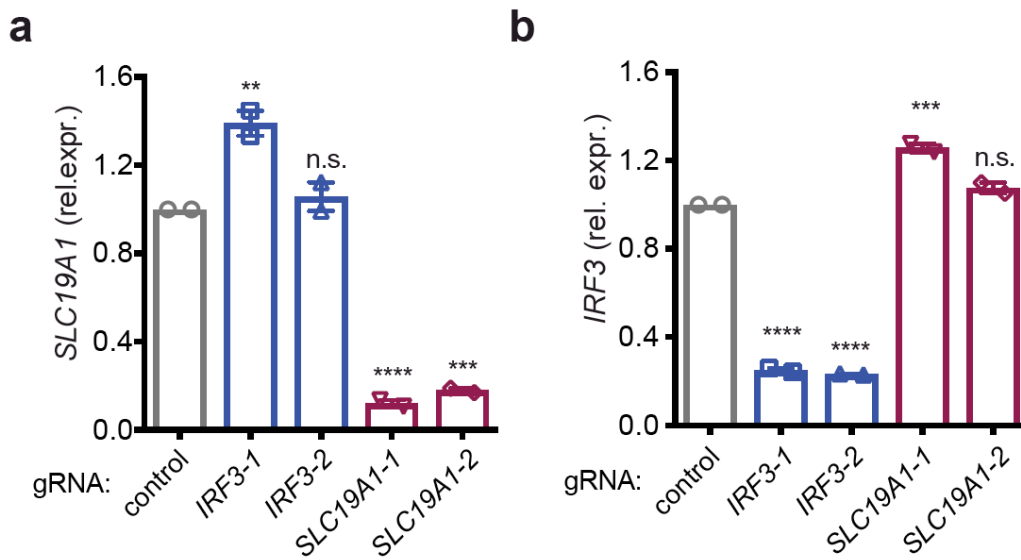
Figure S4. SLC19A1 is critical for CDN-induced reporter expression. a,b, mRNA expression levels of (a) *SLC19A1* or (b) *IRF3* in THP-1 cells expressing a CRISPRi vector and a control non-targeting gRNA or gRNAs targeting IRF3 or SLC19A1 (two gRNAs each). Error bars represent ± SEM of at two biological replicates. Statistical analysis was performed to compare each cell line to the control using a one-way ANOVA followed by Dunnetts's post-test. ***$P \leq 0.001$; ****$P \leq 0.0001$; n.s. not significant.

Figure S5

Signalling induced by CDNs:
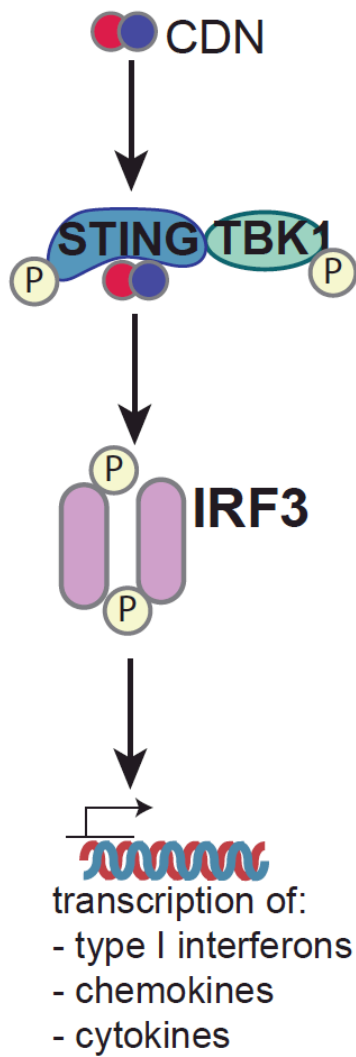
Figure S5. Schematic overview of CDN-induced phosphorylation (P) of STING and downstream effectors TBK1 and IRF3.

Figure S6
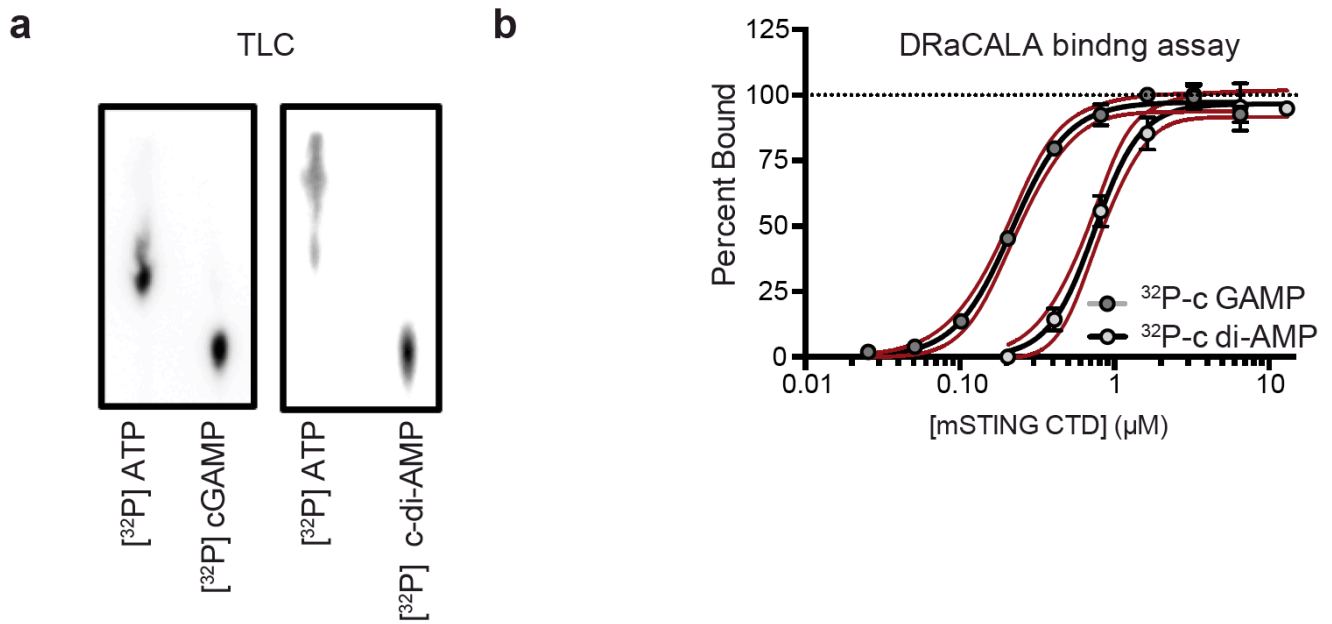
Figure S6. Analysis of enzymatically generated [^{32}P] cyclic dinucleotides. **a,** Thin layer chromatography (TLC) analysis of [^{32}P] ATP and enzymatically synthesized [^{32}P] 2'3' cGAMP and c di-AMP. **b,** Binding titration of [^{32}P] 2'3' cGAMP or c-di-AMP with mSTING C-Terminal Domain (CTD), determined with DRaCALA assays. Red dashed lines represent the 95% confidence interval for the non-linear regression.

Figure S7
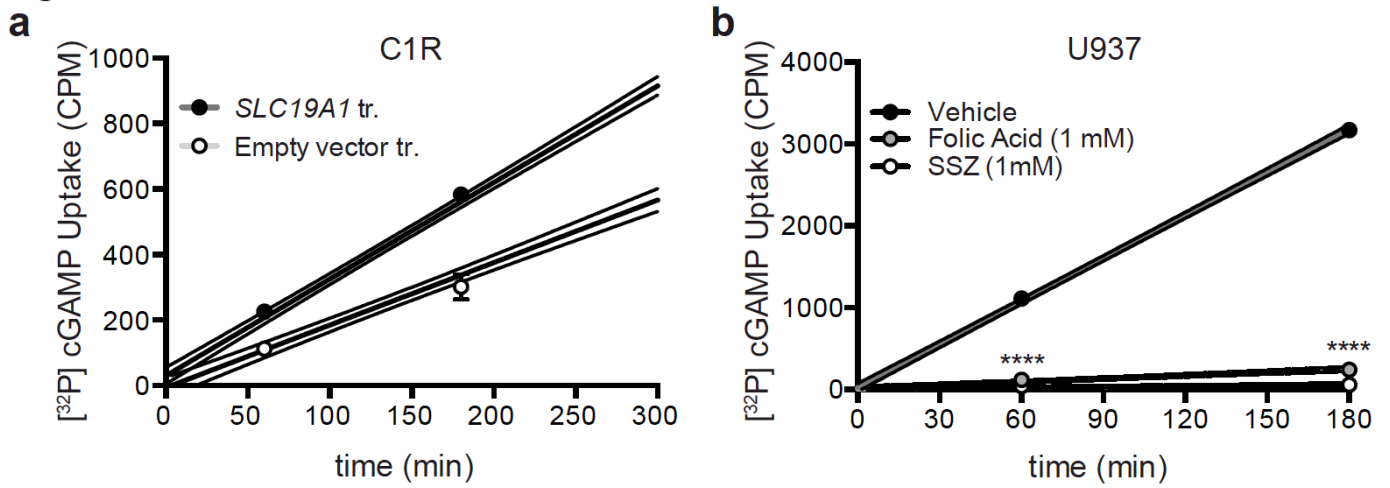
Figure S7. CDN uptake in C1R and U937 cells. **a,** Time course of [^{32}P] 2'3' cGAMP uptake by CIR cells transduced (tr.) with empty vector or *SLC19A1*. **b,** Time course of [^{32}P] 2'3' cGAMP uptake by U937 monocytes in the presence of excess folic acid or sulfasalazine (SSZ). In all panels, error bars represent ± SD of biological replicates. Dashed lines represent the 95% confidence interval for the non-linear regression. Statistical analysis was performed using a Student's t-test (a) or one-way ANOVA (b) followed by Tukey's post-test. ***$P \leq 0.001$; ****$P \leq 0.0001$

Figure S8
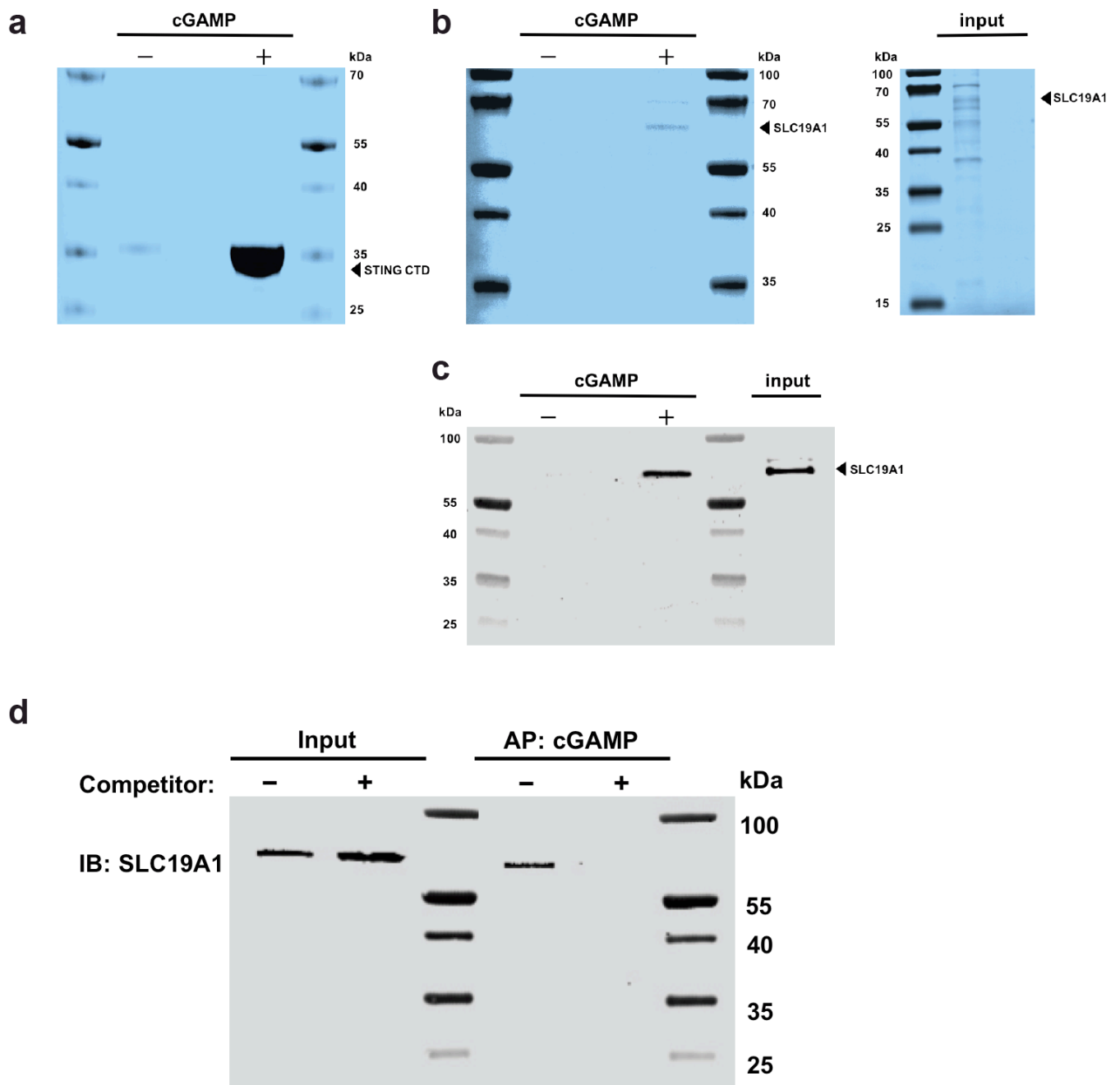
Figure S8. SLC19A1 interacts with 2'3' cGAMP. **a,** Sodium dodecyl sulfate (SDS)-PAGE analysis followed by Coomassie Blue staining of mSTING-C-Terminal Domain (CTD) pull-downs with 2'3 cGAMP (+) or control (−) Sepharose. **b,** SDS-PAGE analysis followed by Coomassie Blue staining of His-tagged hSLC19A1 pull-downs with 2'3' cGAMP (+) or control (−) Sepharose as well as the input material following Ni-NTA affinity purification (right panel). **c,** SDS-PAGE analysis followed by Western blot analysis of His-tagged hSLC19A1 pull-downs with 2'3' cGAMP (+) or control (−) Sepharose as well as the input material following Ni-NTA affinity purification. The two panels were run on the same gel but separated for comparison to the panels in B. **d,** SDS-PAGE analysis followed by Western blot analysis of 8xHis-tagged hSLC19A1 affinity purification (AP) with 2'3' cGAMP Sepharose in the absence (-) and presence (+) of free, unbound 2'3' cGAMP (250 µM).
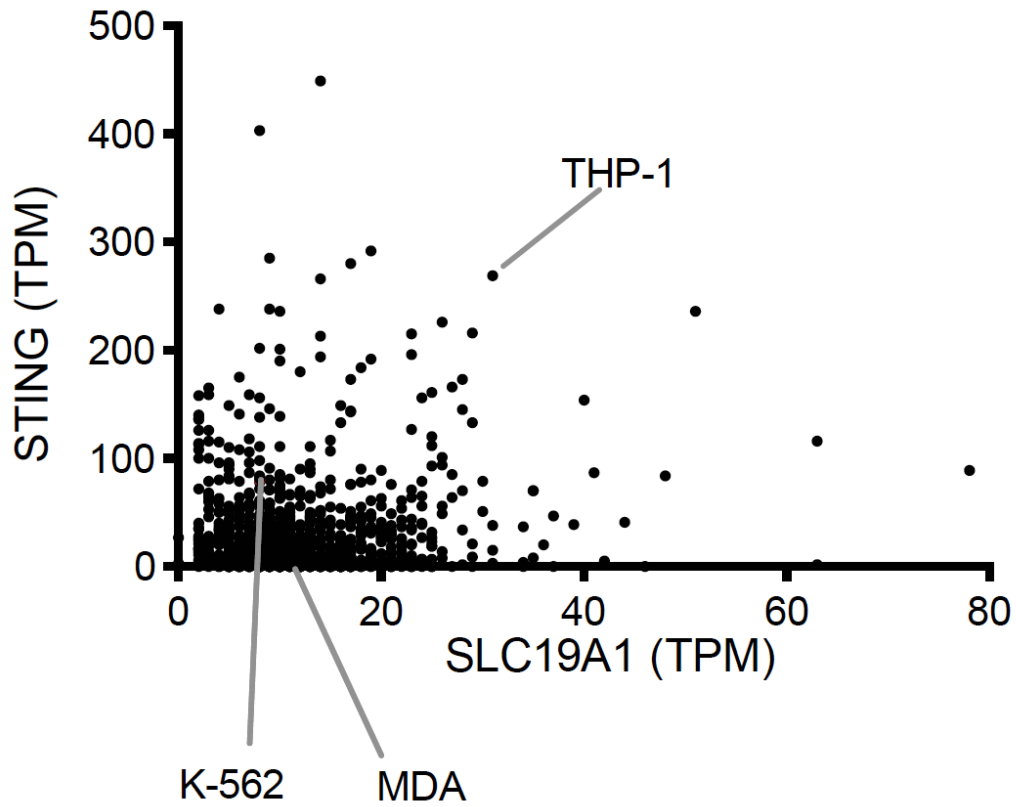
Figure S9

Figure S9. RNA-Seq data of STING and SLC19A1 mRNA expression in 934 human cancer cell lines available at the Cancer Cell Line Encyclopedia. Expression is presented as transcripts per kilobase million (TPM). Data is downloaded from the European Bioinformatics Institute Gene expression Atlas (URL: https://www.ebi.ac.uk/gxa/home). The data set included three of the cell lines we examined, as shown.
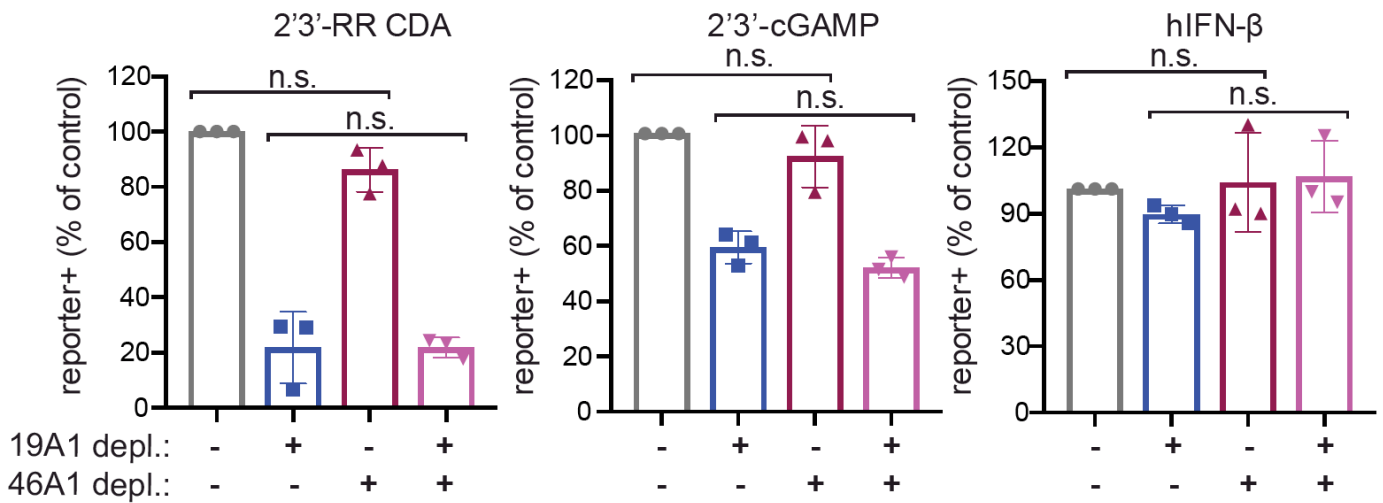
Figure S10
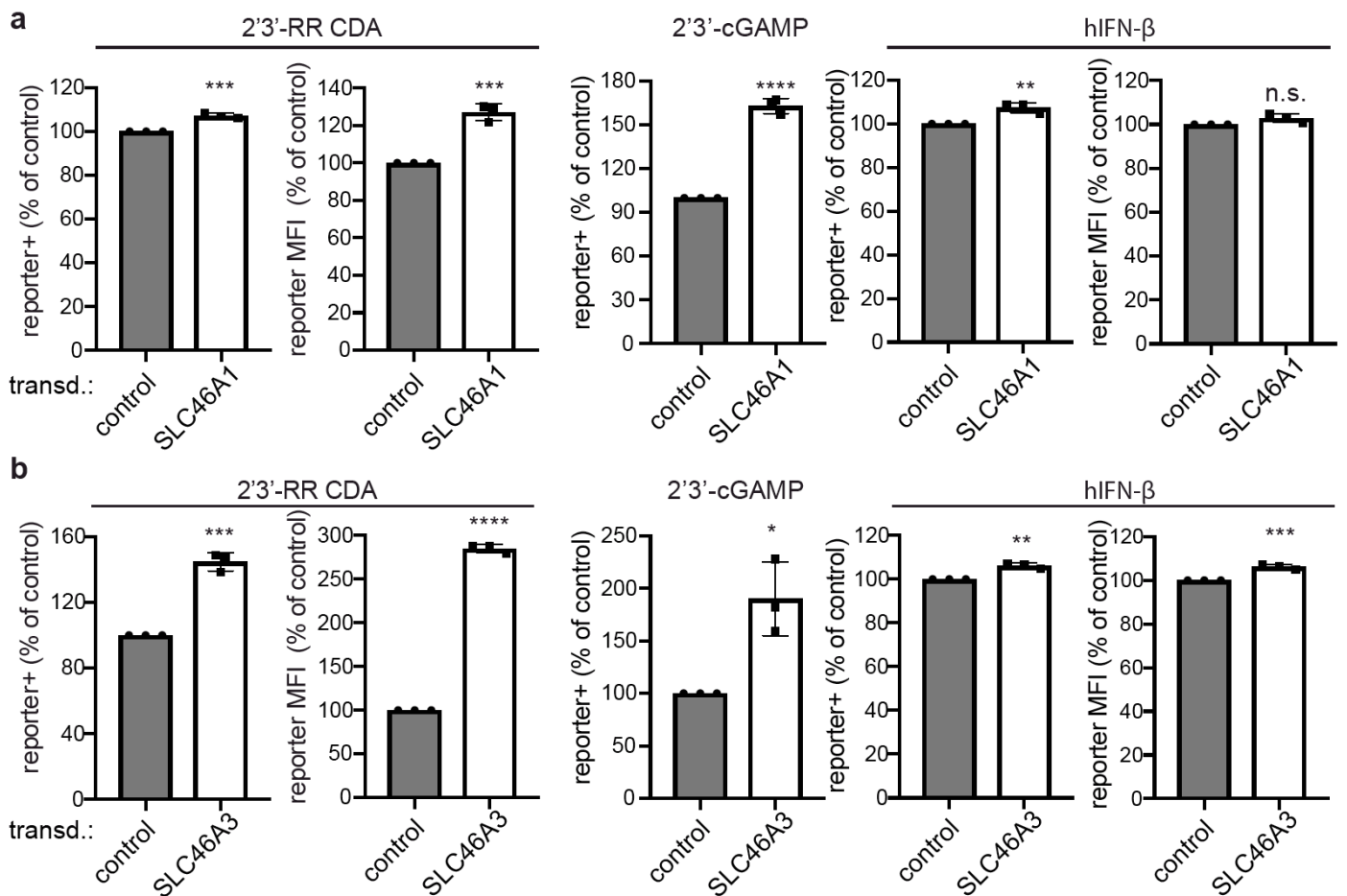
Figure S10. Enforced expression of *SLC46A1* and *SLC46A3* affects the responses of THP-1 cells to CDNs. Control THP-1 cells (transduced with empty expression vector) and *SLC46A1*-transduced THP-1 cells (a) or control THP-1 cells and *SLC46A3*-transduced cells (b) were stimulated with 2'3'-RR CDA (1.25 μg/ml), 2'3'-cGAMP (15 μg/ml) or hIFN-β (100 ng/ml). tdTomato reporter expression was measured by flow cytometry 18-22h after stimulation. Combined data of three independent experiments. Statistical analysis was performed using a two-tailed unpaired Student's t test. Error bars represent ± SEM of independent replicates. *$P \leq 0.05$; **$P \leq 0.01$;***$P \leq 0.001$; ****$P \leq 0.0001$; n.s. not significant.
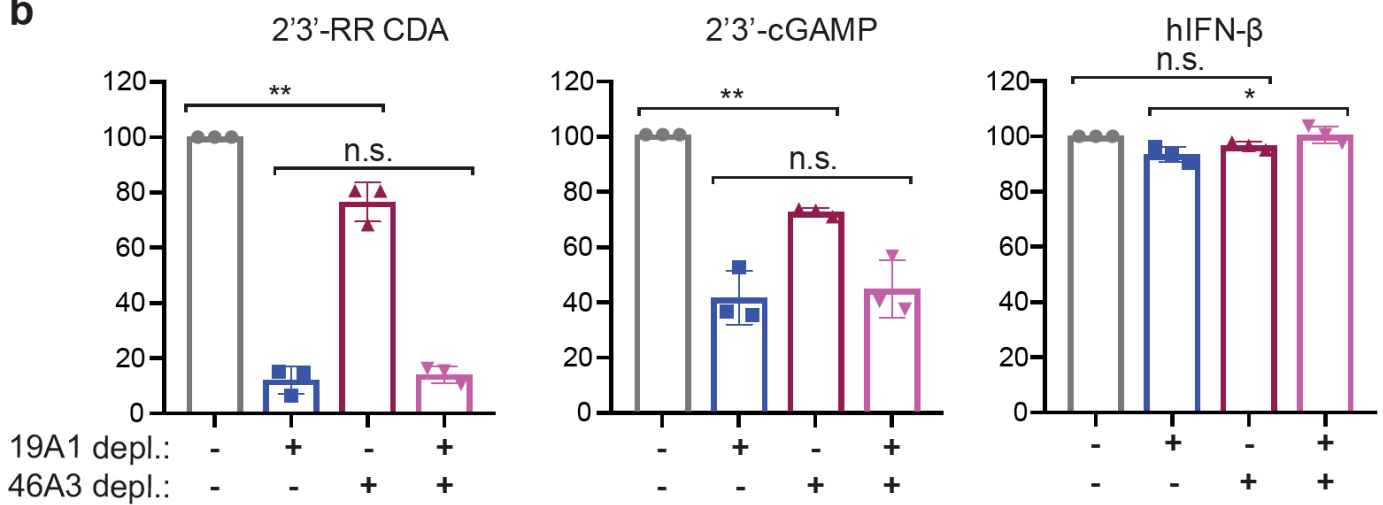
Figure S11. *SLC46A1* or *SLC46A3* depletions, in combination with *SLC19A1* depletion have no additional effect on stimulation by CDNs. THP-1 cells were transduced with non-targeting control CRISPRi gRNAs or *SLC19A1*-targeting CRISPRi gRNA in combination with a second control CRISPRi gRNA or *SLC46A1*-targeting CRISPRi gRNA in (a) or *SLC46A3*-targeting gRNA in (b). Cells were stimulated with 2'3'-RR CDA (1.67 µg/ml), 2'3'-cGAMP (10 µg/ml), or hIFN-β (100 ng/ml). tdTomato reporter expression was measured by flow cytometry 18-22h after stimulation. Combined data of three independent experiments. Statistical analysis was performed using a one-way ANOVA followed by a Tukey's post-test, comparing only the effects of depleting SLC46A1 (a) or SLC46A3 (b). Error bars represent ± SEM of independent replicates. *$P \leq 0.05$; **$P \leq 0.01$; n.s. not significant.